This manuscript is a preprint and has been submitted for publication in **Basin Research**. Please note that this manuscript has not yet undergone peer-review; as such, subsequent version of this manuscript may have different content. We invite you to contact any of the authors directly to comment and give any feedbacks on the manuscripts.

What Controls Contraction in the Translation Domain of the Outer Kwanza Basin, Offshore Angola?

Aurio Erdi
Basin Research Group (BRG), Department of Earth Science and Engineering, Imperial College, London, United Kingdom.
Research Center for Geotechnology, Indonesian Institute of Science, Bandung, Indonesia.
a.erdi18@imperial.ac.uk

Christopher A-L. Jackson
Basin Research Group (BRG), Department of Earth Science and Engineering, Imperial College, London, United Kingdom.
c.jackson@imperial.ac.uk

Corresponding Author
Aurio Erdi
Email: a.erdi18@imperial.ac.uk

Funding Statements/Information
Indonesia Education Scholarship (BPI), Indonesia Endowment Fund for Education (LPDP), Grant/Award Number: 201712220212151

Data Availability Statement
The seismic data supporting the findings of this study are available from CGG. However, restrictions apply to the availability of these data, which were used under license for this study.

ORCID ID
Aurio Erdi
https://orcid.org/0000-0003-4247-715X

Christopher A-L. Jackson
https://orcid.org/0000-0002-8592-9032

Abstract

It is now well-established that base-salt relief drives complex deformation in the mid-slope domain of salt-bearing passive margins, in a location classically thought to be dominated purely by horizontal translation. However, due to a lack of detailed studies drawing on high-quality, 3D seismic reflection data, our understanding of how base-salt relief controls four-dimensional patterns of salt-related deformation in natural systems remains poor. We here use 3D seismic reflection data from, and structural restorations of the Outer Kwanza Basin, offshore Angola to examine the controls on the evolution of variably oriented salt anticlines, rollers, and walls, and related normal and reverse faults. We show that the complex geometries and kinematics of predominantly contractional salt structures reflect up to 22 km of seaward flow of salt and its overburden across prominent base-salt relief. More specifically, contractional deformation occurs where seaward salt flow: (i) is retarded, and salt thickens and overburden buckles above landward-dipping ramps; (ii) encounters thick, slower-moving salt at the base of seaward-dipping ramp; (iii) translates across an array of concave-into-the-basin ramps; (iv) is retarded due to the formation of primary salt welds at the upper hinge of seaward-dipping ramps. The rate at which salt and its overburden translates seaward varies along strike due to corresponding variations in the magnitude of base-salt relief and, at a larger scale, primary salt thickness. As a result, overburden rotation accompanies bulk contraction. Our study improves our understanding of salt-related deformation on passive margins, highlighting the key role of base-salt relief, and showing contraction and rotation are fundamental processes in mid-slope translational domains of salt basins.

Keywords: passive margin, section restoration, salt weld, salt tectonics, shortening, base-salt relief, structural geology

1. Introduction

Salt-bearing passive margins are typically characterised by thin-skinned, gravity-driven deformation that occurs above a salt layer. Kinematically-linked domains of the deformation form, (e.g. Brun & Fort, 2004, 2011; Rowan et al., 2004) with the upslope domain represented by extensional structures such as salt-detached faults and associated salt rollers and rafts (e.g. Duval et al., 1992; Lundin 1992; Rowan et al., 1999; Brun and Mauduit, 2009), whereas the downslope domain is represented by contractional structures such as salt anticlines and salt-detached thrusts (e.g. Cramez and Jackson, 2000; Hudec and Jackson, 2004). These two domains are commonly connected by an intermediary, mid-slope domain (e.g. Cramez and Jackson, 2000; Davison et al. 2012; Quirk et al., 2012; Jackson et al., 2015), which has historically been viewed as a translational zone of relatively little deformation, within which ramp-syncline basins (RSBs) may develop (e.g. Jackson and Hudec, 2005; Peel, 2014; Pichel et al., 2018). In contrast, relatively recent studies using 2D seismic reflection data (or 2D profiles through 3D data) and physical models have demonstrated that the mid-slope domain can be strongly deformed, and can experience multiple phases of extensional and contractional deformation, if the salt and its overburden translate seaward above base-salt relief (e.g. Dooley and Hudec, 2017; Ferrer et al., 2017; Dooley et al., 2017; 2018). Despite offering an improved understanding of the regional kinematics of salt-bearing passive margins, these approaches are limited in that they provide only a two- rather than three-dimensional view. The predictions of physical models also need testing with studies of natural systems.

A recent study by Evans and Jackson (2019) used 3D seismic reflection data from the mid-slope domain of the Outer Kwanza Basin, offshore Angola to show how base-salt relief controlled the temporal and spatial development of ramp-syncline basins (RSBs). Their three-dimensional study of this natural salt-tectonic system also showed how changes in the downdip volumetric flux and velocity of the salt caused local extension or contraction of the salt and its overburden, associated with local acceleration or deceleration of the salt, respectively. This interaction with base-salt relief created locally variable stress fields that deformed the salt and its overburden, overprinting the broader, margin-scale salt tectonics typically associated with gravity gliding and spreading. Evans and Jackson (2019) also suggest that an along-strike (to the SE) increase in regional salt thickness resulted in the salt and its overburden translating seaward more quickly in that direction. As a result, ramp-syncline basins and associated salt diapirs were rotated clockwise during translation. Their study, however, did not establish how specific base-salt structural configurations controlled specific salt-related structural styles, nor spatial variations in the rate of seaward translation of the salt and its overburden in the mid-slope domain.

Our study develops the ideas presented and uses the kinematic framework defined by Evans and Jackson (2019) from the Kwanza Basin, offshore Angola to show that the mid-slope translational domain can be strongly deformed in response to multiphase extension and contraction. As predicted by physical models, this complex deformation relates to the translation of salt and its overburden above base-salt relief. Our high-quality 3D seismic reflection dataset allows us to examine the spatial distribution of and relationship between base-salt relief, salt thickness and salt structural style, and the supra-salt structural framework. By restorating sub-regional seismic profiles, we identify the impact these relationships have on the location and rate of seaward translation of salt and its overburden. Furthermore, we demonstrate that base-salt relief and the formation of primary salt weld are keys control on the geometry, distribution, and kinematics of contractional structures in the mid-slope domain of salt basins.

2. Geological Setting

The Outer Kwanza Basin is an offshore sub-basin of the Kwanza Basin, Angola (Fig. 1a) (Lundin, 1992; Brownfield, 2006; Jackson and Hudec, 2009). The basin is separated from the Inner Kwanza Basin by a basement-cored high called the Flamingo Platform, and is bound at its western end by the Angola Abyssal Plain and at its southern end by several volcanic seamounts. To the north, the Outer Kwanza Basin transitions into the Lower Congo Basin (Hudec and Jackson, 2002; 2004; Jackson and Hudec, 2005; Brownfield, 2006).

The Kwanza Basin initially formed during the Early Cretaceous rifting associated with the opening of the South Atlantic Ocean (Fig. 2). Rifting is recorded by the development of N-to-NW-trending oceanic ridges, a NE-trending transform margin, and the formation of numerous horst-and-graben systems in the present offshore area (Karner and Driscoll, 1999; Hudec and Jackson, 2002, 2004; Brownfield and Charpentier, 2006; Guiraud et al., 2010; Serié et al., 2015). During the latter stages of rifting, in response to the onset of more restricted marine conditions, a thick (up to 1.4 km), Aptian salt-dominated unit was deposited, draping residual rift-related basement highs and thickening southward (Marton, 2000; von Nicolai, 2011; Evans and Jackson, 2019). The salt is presently relatively thick in the Outer Kwanza Basin, gradually thinning eastward onto the Flamingo Platform, where it is locally absent (Hudec and Jackson, 2002; 2004; Karner et al., 2003; Jackson and Hudec, 2005).

Aptian salt controlled post-rift, gravity-driven deformation and the overall tectono-stratigraphic evolution of post-Aptian sequences in the Outer Kwanza Basin (Duval et al., 1992; Lundin, 1992; Marton et al., 2000; Quirk et al., 2012). This gravity-driven salt-tectonic system comprises kinematically-linked zones of updip extension above the Flamingo Platform and downdip contraction towards the seaward edge of the salt (Fig. 1b) (Hudec and Jackson, 2002; Hudec and Jackson, 2004). The intervening zone of bulk translation is defined by a range of structural styles that appear to define four main kinematic phases (Fig. 2) (Evans and Jackson, 2019). First, during the Albian, local contractional and extensional deformations occurred due to salt flow across a series of base-salt ramps, resulting in the formation of salt anticlines and rollers. Second, during the Cenomanian to Oligocene, regional tilting of the margin, driven by post-rift thermal subsidence focused along the western edge of the Outer Kwanza Basin, occurred. This initiated regional overburden gliding and translation and locally rotation above base-salt relief. During this phase, salt flow across base-salt highs generated overburden extension and the formation of rafts, and locally, where contraction occurred, salt anticlines. Third, during the Oligocene and Miocene, salt-detached seaward translation and rotation of the overburden continued. Local extension drove reactive diapirism and the rise of salt walls, in some cases by the breaching of the roofs of previously formed salt anticlines. Elsewhere, in contractional strain fields, some pre-existing structures were locally shortened. Finally, uplift of the African continent during the Miocene to Recent continued to drive seaward translation and rotation of salt and its overburden, but at an accelerated rate. Translation, and local shortening and rotation caused squeezing and active rise of some salt walls. Salt welding, and an increase in sediment accumulation rate relative to diapir rise rate, eventually led to the burial of salt structures and a decrease in margin-scale salt tectonics.

We focus on an area located between the basin-margin rift-related horsts and a large transform fault (Fig. 1a, b) (i.e. the ‘monocline’ and ‘diapir’ domain of Hudec and Jackson, 2004; see also Guiraud et al., 2010). The monocline domain contains RSBs formed due to the seaward translation of salt and its overburden (e.g. Jackson and Hudec, 2005; Dooley et al., 2017; 2018; Pichel et al., 2018; 2019; Evans and Jackson, 2019). By analysing these RSBs and flanking salt structures, Evans and Jackson (2019) show that overburden in this area underwent c. 23 km of seaward translation and a clockwise rotation of c. 32^{o}. The diapir domain contains a range of salt structures formed in response to extension and contraction (i.e. salt anticlines, rollers, walls, and sheets) (Hudec and Jackson, 2004; Evans and Jackson, 2019).

3. Dataset and method

3.1 Datasets and seismic interpretation

This study uses 1276 km^2 of a 2,915 km^2, zero-phase processed, post-stack depth migrated (PSDM) BroadSeis^{TM} 3D seismic dataset that covers the Outer Kwanza Basin, offshore Angola (Fig. 1a, b). Due to confidentiality reasons, the data are cropped at the base-salt (c. -5.5 km). However, the morphology of the base-salt surface, which controls many of the salt-related structural styles documented here and by Evans and Jackson (2019), is clear. This dataset has inline (northwest-southeast) and crossline (northeast-southwest) spacing of 25 m; inlines and crosslines are oriented broadly normal and perpendicular to the bulk south-westerly translation direction, respectively. The seismic dataset has a record length of 10 km and a vertical sample rate of 2 m, with a vertical resolution of c. 3.5 m and c. 30 m at the seabed and at a depth of c. 5 km, respectively. These data are displayed with the Society of Economic Geologist (SEG) 'normal' polarity convention; i.e. a downward increase and decrease in acoustic impedance are represented by a positive reflection (white) and a negative (black) reflection event, respectively. We mapped eight seismic horizons, the ages of which are constrained by comparing our data to age-constrained regional seismic profiles presented by other authors (Table 1). Age constraints allow us to establish the relative timing of different salt-tectonic events by identifying key seismic-stratigraphic surfaces (e.g. onlap, truncation).

3.2 Restoration analysis

Semi-quantitative structural restorations were undertaken using 2DMove©. We restored cross-sections oriented broadly parallel to the regional (salt) tectonic transport direction in order to: (i) validate our seismic interpretation; (ii) unravel the two-dimensional evolution of salt-related local contractional structures; and (iii) calculate spatial variations in the magnitude of seaward translation and rotation of the suprasalt (see Appendix A.1 for full detail information of all restoration of these cross sections, methodology, and algorithms). A key constraint on our structural restoration were the RSBs, which are inferred to initiate at the top of fixed (i.e. static) ramps present along the base-salt (cf. Hudec and Jackson, 2004; Jackson and Hudec, 2005; Rowan and Ratliff, 2012). We also used observations from physical models to determine the likely temporal and spatial relationship between base-salt structures, and the structures present in the salt and its overburden (Fig. 3a, b) (Dooley and Hudec, 2017; Dooley et al. 2017; 2018; see Appendix A.2 for additional details).

4. Base-salt structural style

We first describe the morphology of the base-salt; this provides a spatial framework for understanding the base-salt-induced deformation identified within the salt and its overburden (Fig. 4a). The base-salt dips broadly to the SW. Superimposed on this are three distinctive trends defined by relatively steeply dipping ramps. In the northeast, the ramps trend NW, are *c.* 13-km long, and define part of the seaward edge of the Flamingo Platform (Fig. 1a, b). In the southwest, the ramps also trend NW, which when combined with the N-trending ramps located in the south, form an array of concave, seaward-dipping ramps (Fig 4a). These two areas are separated by four sub-rectangular-to-sub-triangular structural highs defining local relief of *c*. 500-1000 m. These four highs trend NW-to-N, face towards landward and seaward-facing of *c.* dip of 14^{o}-40^{o}, (V, W, X, Y and Z; Figs 5a, 6a, b, 7, and 8). These local sub-salt structural highs and associated ramps may be related to the Angola-Gabon horst-block system (*sensu* Hudec and Jackson, 2004), although our lack of sub-salt seismic imaging means we cannot establish if the highs are definitely fault-bounded. In the north and the southeast, we observe relatively short (<11 km long) NE-trending ramps that face either SE or NW, and which locally intersect a NW-trending ramp (Figs 4a). These NE-trending ramps are consistent with the trend of the Martin Vaz transfer fault zone (Fig. 1a) (*sensu* Moulin et al., 2005; Guiraud et al., 2010); we thus infer these ramps are the upper crustal expression of this lithosphere-scale structure.

5. Distribution and Style of Salt and Supra-salt Structures

The geometry of salt and supra-salt structures vary across the study area. A salt-thickness map allows us to define distributions of the salt structures we infer are related purely to contractional (e.g. salt anticlines), and other structures of more variable origin (e.g. salt walls) (Table 2; Figs 5-7). Some salt structures are separated by apparent primary welds (*sensu* Wagner and Jackson, 2011), across which supra-salt strata appear to directly overlie sub-salt strata (Fig. 7b, c). A structure map of the Albian seismic horizon, which records cumulative translation of the overburden, defines the *present* spatial relationships between salt and spatially related supra-salt structures (e.g. salt-detached normal faults, outer-arc bending normal faults, and thrusts and strike-slip faults; Table 3; Figs 5, 6, and 7). As indicated by Evans and Jackson (2019), it is critical to note that: (i) the salt and supra-salt structures are unlikely to be in the same position as where they formed, given they have translated seaward a few tens of kilometres; and (ii) the *present* spatial relationship between the salt and supra-salt structures, and the underlying base-salt structures, is unlikely to causal. Finally, the salt, and supra-salt faults and thrusts, are overlaid by and occur within RSBs that formed purely in response to Eocene-to-Pliocene, salt-detached translation of the overburden (Figs 6 and 7b, c). However, as shown by Pichel et al. (2018), we note that RSBs can be internally deformed by post-formation diapirism and salt-related faulting.

Interpretative sketch maps of the main salt structures (as defined at the top salt structural level), the supra-salt structures (as defined at the Albian structural level), and a simplified base-salt structure map, show the *present* spatial relationship between features at all three levels (Fig. 8). Both the salt and supra-salt structures are varied in terms of their distribution and orientation relative to underlying base-salt ramps that trend predominantly NW, N, or NE. More specifically, salt and supra-salt structures trend either parallel or oblique to these ramps. However, we also observe instances in which salt structures overlie relatively flat regions on the base-of-salt, such as the salt anticlines and contractional salt walls located in the southwest and the south (SC1 and SW2; Fig 5b). We now describe and illustrate the geometry, origin and evolution of salt and salt-related structures, with focus on the kinematics of contractional structures. The evolution of these contractional structures are illustrated by the structural restoration of selected cross-sections (Fig. 9).

6. Salt-related Contractional Structural Style

6.1 Salt anticlines

6.1.1 Geometry

In the southwest, salt anticlines trend broadly parallel to NE-trending, base-salt ramps, or are presently located above relatively flat areas of the base-salt surface (SC1; Fig 8). The anticlines above the flat areas are polyharmonic, increasing in wavelength, but decreasing in amplitude, upwards (SC1; Figs 5b and 7b, c). These salt anticlines are commonly overlaid by relatively thick (up to 800 m) roofs, suggesting they formed in response to contraction (Jackson & Hudec, 2017). In the north, where the ramp changes to trend NW, the anticlines similarly change trend to stay sub-parallel to the underlying structures, being located above either seaward- or landward-facing ramps (SC3-6; Fig. 8). Above seaward-facing ramps, limbs of these salt anticlines are commonly dissected by salt-detached normal faults, such as above the landward limb of SC4 (Fig. 6a), suggesting this anticline may have been later reactivated by extension. From this point northeastward, these salt anticlines are overlaid by thick roofs, underlain by still-thick salt, and have their seaward limbs offset by NW-SE-striking thrusts faults immediately above the downdip end of these ramps (SC5 and SC6; Fig. 6a). In a few cases in the north of the study area, highly-deformed anticlines are presently located above seaward-facing ramps (SS1; Fig. 8a). These anticlines are characterised by a triangular salt pedestal, a secondary weld, and are sometimes overlain by normal faults inferred to be related to outer-arc bending of the arched roof. These features are consistent with a salt anticline that has been amplified and laterally squeezed in response to horizontal shortening (SS1; Fig. 6c).

6.1.3 Structural Evolution

6.1.3.1 Early Cretaceous

The anticline, at least those in the southwest of the study area, initiated relatively early, in the Albian; this is indicated by anticlines that are flanked and overlain by intra-Albian growth strata (SC1; Figs 5b, c, 6b, 7b and c). We suggest the salt anticlines formed due to: (i) buckling at the base of base-salt ramps, as relatively fast-moving thin salt encountered relatively slow-moving thicker salt (Hudec and Jackson, 2005; Evans and Jackson, 2019); and/or (ii) salt thickening, deceleration and overburden shortening upon encountering landward-dipping base-salt ramps (i.e. in cases where the anticlines are presently located on base-salt plateaus (Fig. 3a) (cf. Dooley et al., 2017; 2018; Pichel et al., 2019). The former interpretation is, however, not consistent with several physical models , which predict that, during the early stages of translation, a monocline rather than a salt anticline may form at the base of the base-salt ramp (Gaullier et al., 1993; Dooley and Hudec; 2017; Dooley et al., 2017; 2018). Although it is possible that such a monocline did form and was subsequently translated further seaward before growing into a salt anticline (Hudec and Jackson, 2005), we prefer the latter interpretation, given we consistently see thickened salt immediately seaward of landward-facing ramps (SC5 and SC6; Fig 6a).

Our structural restoration, which are based on the assumption that anticlines form due to translation across the landward- (up-flow) facing side of base-salt highs, suggest salt anticlines in the centre and south of the study area, initiated in the Late Albian in association with local structural highs (cf. Fig. 3a) (ii; Fig. 9a, b). We propose that the polyharmonic geometry of the salt anticlines, such as in the southwest, reflect continuous (rather than protracted) local contraction during overburden thickening (c.f. Fig. 3c) (SC1; Figs 5b, c and 7b, c).

6.1.3.2 Late Cretaceous-Paleogene

During the Eocene to Oligocene, new salt anticlines initiated, and established, Early Cretaceous anticlines amplified, as indicated by their association with Eocene-to-Oligocene growth strata. This observation shows that base-salt relief-related overburden shortening was diachronous across the study area, with salt anticlines starting to grow in the SW during Eocene, becoming younger and more deformed towards the NE (c.f. SC1; Figs 5b, 6b and 7b, c and SC4-6; Fig. 6a).

Our restoration in the north reconstructs the Late Cretaceous-Paleogene location of the salt anticlines, suggesting that diachronous growth of the salt anticlines was again associated with salt flow and overburden translation over local base-salt highs (ii-iv; Fig. 9c). More specifically, we see three key phases in the growth of anticlines at this times: (i) initiation of anticline growth due to the seaward flow of salt and overburden over landward-facing ramps in the Late Cretaceous-Early Eocene (ii; Fig. 9c) (cf. Fig.3a); (ii) local extensional faulting of the anticlines in the Late Eocene as they translated across the seaward-facing ramps (iii; Fig. 9c) (c.f. labelled 2; Fig. 3b); and (iii) further seaward translation of anticlines during the Oligocene, and formation of seaward-verging thrusts as the salt and overburden passed over landward-facing ramps (iv, Fig. 9c).

6.1.3.3 Neogene-Present

During the Miocene to Holocene, some pre-existing anticlines were locally influenced by contraction. For example, in the southwest, Middle Miocene strata onlap onto underlying strata and are dissected by outer-arc bending-related normal faults above salt anticlines, showing that, during Miocene-Holocene translation, salt anticlines were laterally squeezed (SS1; Figs 5d and 6c). We suspect that this squeezing may reflect the contraction of the salt anticlines at the base of the seaward-facing ramps as they passed through the contractional hinge (c.f. labelled 3; Fig. 3b).

6.2. Salt walls

6.2.1 Geometry

Salt walls broadly trend either parallel or oblique to NW-, N-trending ramps, being presently located above either the relatively flat parts of the base-salt or landward-facing ramps (SW1-5 and SS2; Fig. 8a). Some salt walls have a triangular profile and a well-defined, pointed crest, and are flanked by inward-dipping, salt-detached normal faults, geometries characteristic of reactive diapirism initiated by overburden extension (SW1 and SW5; Fig. 5a) (e.g. Vendeville and Jackson, 1992a). In contrast to the morphologically and genetically, somewhat simple reactive diapirs, we observe two additional types of rather more complex salt walls in the centre and the northeast of the study area (SS2, SW2, SW3 and SW4; Figs 6b, c and 7).

The first type are represented by walls that vary in terms of their map-view trend and overall geometry, and which have variable spatial relationships with base-salt ramps (SW2; Fig. 8a). In the centre and the south of the study area, SW2 trends parallel to and is presently located downdip of NW-trending, seaward-facing ramps, or relatively flat areas immediately seaward of these ramps (SW2; Fig. 7 b, c). Similar to the triangular salt walls described above, SW2 has a triangular profile and is flanked by inward-dipping, salt-detached normal faults. However, near its centre, SW2 has a rounded rather than pointed crest, whereas in the south where the crest is pointed, the flanking faults have relatively shallow dips (<50°). Based on these geometrical characteristics, we infer that these walls formed as reactive diapirs, with their latter growth occurring in response to horizontal shortening (e.g. Vendeville and Jackson, 1992b). This shortening drove roof arching, rounding-off of the diapir crest, and the passive rotation of normal faults to lower structural dips. The northern end of SW2 presently trends parallel to and is located above-to-slightly downdip of, a seaward-facing ramp (SW2; Fig. 7a). Here, SW2 is capped by an irregular, indented crest, which is associated with a salt horn. By comparison to geometries formed in physical models, we infer that this distinctive structural style formed in response to extension-driven diapir fall, possibly related to the flow of salt along strike within the wall to feed another part of the structure that was actively rising due to synchronous shortening (SW2; Fig. 5d) (e.g. Vendeville and Jackson, 1992a).

The second type of salt walls are represented by structures trending parallel to, and being presently located above or slightly downdip of, NW-trending, seaward-facing ramps, or the relatively flat areas immediately seaward of these ramps (SS2, SW3 and SW4; Fig. 8a). At its northern end, SS2 is presently located above a relatively flat part of the base-salt. In this location, SS2 is flanked by inward-dipping faults overlying a triangular salt pedestal, a secondary weld, and an arched roof (Fig. 6c), features characteristic of a reactive salt wall that was subsequently squeezed (c.f. Vendeville and Nilsen, 1993; Rowan et al., 2004; Jackson et al., 2008; Dooley et al., 2009). We observe another two walls of this complex type in the northeast of the study area; these structures, which are separated by a primary weld and which overlie a NW-trending, seaward-facing base-salt ramp, are both geometrically similar to SS2, but are both characterised by thrusted roofs (SW3 and SW4; Fig. 7a). Here, at the base of this ramp, SW4 is characterised by a very well-defined triangular profile, is flanked by inward-dipping faults, and a NW-SE-striking, landward-dipping thrust above its crest (SW4; Fig. 7a). However, further to the northwest, SW4 appears to be overlain by outer-arc bending-related normal faults being located above a rollover monocline (see Fig. 6b). Thrusts, similar to those observed further to the southeast, are not developed. Based on these characteristics we suggest that the rollover monocline was draped over the western flank of the SW4, which originally formed as a reactive diapir, inducing the formation of outer-arc bending-related normal faults in its roof; the structure and its overburden were subsequently shortened, and related faults reactivated to form the crestal fore-thrust.

6.2.3 Structural Evolution

6.2.3.1 Late Cretaceous-Paleogene

The age of growth strata indicate salt walls began to grow in the Eocene to Oligocene. For example, Late Cretaceous-to-Eocene strata locally onlap onto underlying (Albian) strata and fill RSBs (Figs 7b and c) or thicken across reactive diapir-flanking faults (SW1; Fig. 5a; SW2; Fig. 7a). Oligocene strata are also locally contained in RSBs. Locally, however, Late Cretaceous-to-Oligocene strata are upturned against and are tabular against diapir flanks, suggesting these structures are younger and that reactive diapir growth was diachronous (SW3, SW4; Fig. 7a and SW2; Fig. 7b, c).

Our structural restorations show that in the north and the centre of the study area, Albian salt anticlines had by the Eocene-Oligocene, translated seaward onto either the flat-topped structural highs or seaward-facing ramps, resulting in crestal extension and the formation of reactive salt walls (SW2-4 in iii-iv; Fig. 9a, b). Based on our restorations, we propose two mechanisms may have caused local overburden extension and reactive diapir rise. First, an increase in the velocity of the seaward flow above the local structural high resulted in the widening of a pre-existing salt anticline, and the formation of extensional faults in its overburden (labelled 1; Fig. 3b) (see late-stage buildup of thick salt body above high block of Jackson and Hudec, 2017; see also Dooley et al., 2017; 2018). Second, the seaward flow of salt was retarded as salt thinned above and at the base of the seaward-facing ramp, resulting in overburden extension (labelled 2; Fig. 3b) (see extensional hinge of Jackson and Hudec, 2017; see also Dooley et al., 2017; 2018). Whichever mechanism we prefer, our key interpretation is that seaward-translating, pre-existing anticlines underwent subsequent extension to become reactive diapirs in the Late Cretaceous-Oligocene. Local contraction did occur in the Oligocene, as evidenced by local arching and thinning of Oligocene strata over walls like SS2 (Fig. 6c). We suggest that contraction was driven by translation of the walls onto the base of the seaward-facing ramps, where they encountered relatively thick, slower-moving salt (labelled 3; Fig. 3b) (see contractional hinge of Jackson and Hudec, 2017; see also Dooley et al., 2017; 2018).

6.2.3.2 Neogene-Present

By the Miocene, salt and its overburden had translated a significant distance seaward (11-21 km; Fig 10); this is comparable to the distance calculated by Evans and Jackson (2019) based on their study of ramp-syncline basins in the SE of the study area (18 km). This translation is recorded in the formation of RSBs (Pichel et al., 2018) and resulted in the continuous growth and/or local contraction of pre-existing diapirs as they passed over base-salt relief (Figs 6 and 7).

During the Early-Middle Miocene, SW3 and SW4 continued to grow, followed by shortening and squeezing at the end of the Middle Miocene. The continued growth of these pre-existing walls by reactive diapirism is indicated by presence of an upturned collar of broadly tabular Early-Middle Miocene strata, which thicken across flanking, salt-detached normal faults (SW3-4; Fig. 7a). Shortening is recorded by the top-truncation of Middle Miocene succession across the diapirs.

Our restoration shows that, during the Early-Middle Miocene, pre-existing (reactive) salt walls continued to grow (SW3-SW4 in v; Fig. 9b). We speculate that the continued growth of these pre-existing walls was influenced by local extensions above the seaward-facing ramps (c.f. labelled 2; Fig. 3b). Furthermore, at the end of the Middle Miocene, whereas some salt walls continued to grow, SW4 continued translating seaward before undergoing contraction at the base of a seaward-facing ramp, reverse reactivating the former salt-detached normal fault responsible for its growth, into a fore-thrust (vi; Fig. 9b) (c.f. labelled 3; Fig. 3b).

During the Late Miocene, shortening continued to occur on SW3 and SW4. The shortening is reflected by thinning of Upper Miocene strata across the thrust-bound block capping the diapirs (SW3-4; Fig. 7a). Our restoration shows that a primary weld formed above a local structural high, whilst SW3 and SW4 were squeezed at the base and top, respectively, of the seaward-facing ramps (vii; Fig. 9b). At the base of the ramp, squeezing caused rotation and welding of the eastern flank of the SW4, whereas further updip this caused reverse reactivation of a salt-detached normal fault above SW3, causing it to now resemble a back-thrust. Three possible mechanisms might plausibly account for generating local contraction and this change in structural style during the Late Miocene. The first relates to retardation of the seaward flow of salt as it encounters local base-salt highs; this could have caused salt thickening, overburden shortening, and fault inversion (cf. Ferrer et al., 2017). However, this interpretation is considered unlikely because, from this point northwestward, salt-detached normal faults rather than thrusts are presently observed above many salt structures (Figs 6b and 8b). As such, the local base-salt high does not appear to have driven the repeated inversion of normal faults to form back-thrust as the salt structures translated seaward above seaward-facing ramps. The second mechanism might somehow reflect slowing of salt and shortening of its overburden as they travel onto a seaward-facing ramp (c.f. labelled 3; Fig. 3b). While this may reasonably explain the generation of the fore-thrust, it is considered unlikely as a more general mechanism because local contraction above seaward-facing ramps has not been documented in physical models; i.e. salt flow onto a downflow-facing ramp induces contraction rather than extension (labelled 2; Fig. 3b) (c.f. Jackson and Hudec, 2017; Dooley et al., 2017; 2018).

Given the spatial relationship between base-salt structures, salt walls, and supra-salt faults during the Late Miocene, inferred from our structural restorations, we suggest shortening and thrusting were driven by a combination of the second mechanism outlined above and primary welding above the seaward-dipping ramp. We interpret that while the growth of the fore-thrust was associated with local contraction at the base of the ramp, the updip weld act as a buttress that inhibited further seaward flow of salt, resulting in overburden shortening and inversion of the former salt-detached normal fault. Our interpretation is consistent with the predictions of physical models, which indicate that salt pinch-out above downflow-facing ramps can induce overburden shortening and thrusting (c.f. Dooley, et al., 2007).

During the Miocene, SW2 was subjected to active rise in the south and extension-driven fall in the centre. In the south, active rise initiated in the Early Miocene; this is indicated by the onlap of Early Miocene strata onto Oligocene strata adjacent to SW2 (Figs 7b and c). Active rise continued during the Middle-Late Miocene, as reflected by overall thinning of upturned Middle-Late Miocene strata against the diapir flank, suggesting it formed a bathymetric high during the Middle-to-Late Miocene. In the centre, however, extension-driven fall initiated in the Middle Miocene, as indicated by the Middle Miocene strata draping over a relic horn at the crest of the northern margin of SW2 (Figs 5d). Extension-driven fall continued into the Late Miocene, as indicated by thickening of Late Miocene strata across normal faults in the diapir roof (SW2; Figs 5d and 7a).

Our structural restorations in the central and southern parts of the study area highlight the temporal evolution of SW2 during the Miocene. In the south, SW2 underwent active rise as it entered a contractional stress field at the base of a seaward-facing ramp (v-vii; Fig. 9a). In contrast, in the centre, SW2 underwent initially extension-driven reactive rise as the diapir travelled onto a seaward-facing ramp and went through the extensional hinge (FIG), and then extension-driven fall (v-vii; Fig. 9b). We suggest that diapir fall was associated with the along-strike flow of salt from the northern part of SW2 in the centre to feed actively rising portions of the wall in the south (c.f. Vendeville and Jackson, 1992b).

By the Pliocene-Recent, some walls were inactive and completely buried, whereas others continued to be grow via shortening-induced active diapirism or extension-driven reactive diapirism. Synchronous shortening and extension is well-illustrated in the centre of the study area, where Pliocene-to-Recent growth strata thin onto an inversion-related fold above SW3, whilst at the same time thickening across salt-detached normal faults on the eastern flank of SW2 (Fig. 7a). In the south, however, Pliocene-to-Recent strata are folded and eroded above SW2, with Late Miocene strata presently exposed at the seabed (Fig. 7b). This observation indicates that locally at least, SW2 continues to actively rise. This is likely driven by ongoing translation, an interpretation consistent with the observation that Pliocene-to-Recent strata fill still-active RSBs (Fig. 7b).

7. Regional Translation Magnitudes and Variability

Having described the geometry, kinematics and possible origin of salt-related structures in the mid-slope domain of the Outer Kwanza Basin, with a focus on the role of base-salt relief, we now use our sub-regional structural restorations to focus on how the magnitude of translation varied along strike (Fig. 10). Based on these restorations we make three key observations related to these variations and how the influenced the geometry and evolution of salt-related structures in three-dimensions.

Our first observation is that the initiation of salt tectonics varied along-strike, commencing in the Late Albian in the centre and south, with approximately 3.7 and 10.5 km of translation being recorded, respectively. In contrast, the northern domain was static until the Cenomanian (D-D', F-F' and I-I'; Fig. 10). These differences are expressed in timing of onset of salt anticlines growth (i.e. Albian in the centre and south, and Eocene in the north; ii; Fig. 9a, b, c). The cause of this variability is not obvious, but it might reflect the fact that Aptian salt was thicker and, therefore, possibly faster flowing in the south (von Nicolai, 2011; Evans and Jackson, 2019). Regardless of the cause, one kinematic consequence of this variability is that the salt and its overburden may have been mildly sheared, undergoing a clockwise rotation.

The second observation is, during the Oligocene, the total magnitude of the translation in the north, where translation did not until the Eocene, surpassed that in the centre, where the translation started earlier (i.e. Late Albian) (D-D', F-F'; Fig. 10). Along-strike variations in the magnitude of translation were accommodated by the local growth of strike-slip faults that are particularly well-developed in the north (Fig. 5a, d and Table 3).

The third observation is that along-strike (i.e. between-domain) variations in translation magnitude continued from the during Oligocene until the Present, and that within domains the rate varied. The variations are clearly shown in the Miocene, when the translation rate was relatively stable in the north, but accelerated in the centre and south. These variations likely reflect along-strike changes in salt thickness, and the interaction between the salt, its overburden deformation, and the base-salt relief.

Our study shows that total absolute translation magnitudes varied along-strike of this segment of this salt-based passive margin (i.e. 13, 11, and 22 km in the north, centre, and south, respectively; Fig. 10). These magnitudes values are generally less than that calculated by Evans and Jackson (2019), based on their analysis of RSBs and flanking salt walls slightly further SE along the margin (i.e. 23 km). We suggest two interpretations might plausibly account for the differences in these magnitude values: (i) salt was originally thicker in the SE, meaning the salt and its overburden flowed seaward relatively quickly compared to the NW (von Nicolai, 2011; Evans and Jackson, 2019); (ii) differences in the magnitude of base-salt relief, being significant in the north and the centre, where the translation magnitude was less, and more subdued in the southeast, where the magnitude was greater (Fig. 4a) (see Dooley et al., 2017; Dooley and Hudec, 2017).

8. Tectonic Evolution of the Mid-Slope Domain, Outer Kwanza Basin

We now link our: (i) detailed analysis of the geometry and evolution of salt-related structures in the context of base-salt relief; with (ii) sub-regional structural restorations that constrain the magnitude of seaward translation to generate eight sequential maps illustrating the three-dimensional, salt-tectonic evolution of the mid-slope domain of this segment of the Outer Kwanza Basin, offshore Angola (Fig. 11). One of the key aims of these maps is to show the initial (i.e. Early Albian) location of salt and supra-salt structures relative to base-salt features, and their subsequent evolution as they translated seaward. For ease of description, these maps are grouped into three main salt-tectonics phases (i.e. Early Cretaceous, Late Cretaceous-Paleogene, and Neogene-Present).

8.1 Early Cretaceous

The Early Cretaceous was characterised by base-salt relief-induced folding of the overburden in the south and centre due to spatial and temporal variations in the rate of seaward salt flow (Fig.

11a). It is likely that translation was triggered by differential thermal subsidence and tilting of the margin after continental break-up (e.g. Hudec and Jackson, 2004). Clockwise rotation of the overburden in the Late Albian occurred due to the fact that translation did not initiate in the north until the Eocene (Fig. 11b).

8.2 Late Cretaceous-Paleogene

The Late Cretaceous-Paleogene was dominated by reactive diapirism and salt wall formation, with this being particularly common in the centre and the northeast due to increasing salt flow velocity above either local structural highs (i.e. flat-topped) or the outer-edge of the Flamingo Platform (i.e. seaward-facing ramps), (Fig. 11 b, c). Local shortening in the north initiated the growth of salt anticlines above the landward-facing ramps, and in the southwest, where the precursor anticlines amplified as they rotated across concave-into-the basin, seaward-dipping ramps. Anticline rotation meant that these structures presently have a wide range of trends (c.f. convergent gliding pattern of Cobbold and Szatmari, 1991). Anticline tightening initiated the growth of outer-arc bending-related normal faults in their roofs.

Synchronous extension-driven diapirism and contraction-driven salt-detached folding reflect spatial differences in the rate of seaward translation of the salt and its overburden, which also resulted in the formation of strike-slip faults in the north, and more distributed strain in the form of overburden rotation in the SE (i.e. 23^{o}; Evans and Jackson, 2019) (Fig. 11c). The overburden rotation occurred due to salt flow slow down across local structural high in the centre, whilst salt flow relatively faster in the southeast above relatively subdued relief (Fig 12) (cf. convergence of salt flow across isolated structural highs; Dooley et al., 2018).

8.3 Neogene-Present

Synchronous extension and contraction driven by salt flow across base-salt relief continued into Neogene. In the southwest, outer-arc bending-related normal faults formed at the crest of salt anticlines, due to shortening and tightening of the precursor anticlines (SC1; Fig. 5b and Fig. 11 d, e, f). This shortening can be attributed to the relatively late, upslope migration of contraction, which continues to the present (Brun and Fort, 2004; Fort et al., 2004). However, where anticlines were located above relatively flat areas of the base-of-salt immediately seaward of concave-into-the-basin, seaward-dipping ramps, we propose that anticline shortening was driven by convergent gliding (c.f. Cobbold and Szatmari, 1991). From this point northward and northeastward, squeezing and active rise of pre-existing walls and anticlines occurred, either at the base or top of seaward-facing ramps (Fig. 11 d, e, f). At the same time, local extension induced reactive piercement of the overburden, resulting in the formation of rollers and rafts above the ramp defining the seaward-edge of the Flamingo Platform (vi; Figs 9a and 11e). These local, short length-scale variations between contractional and extensional structures reflect disparities in the magnitude and rate of seaward translation of the salt and its overburden, with this again being accommodated in the north by strike-slip faulting and in the east by more distributed shear (i.e. rotation). Salt tectonics is presently modest in the mid-slope domain, and most salt and supra-salt structures are buried and inactive. Locally, however, active diapiric rise and deformation of the seabed attest to ongoing shortening (Fig. 11g).

9. Controls on Mid-Slope Contractional Salt Tectonics

Classic models of salt-bearing passive margins state that salt-related deformation above relatively smooth base-salt relief are related to the kinematically-linked domains of updip extension, mid-slope translation, and downdip contraction (e.g. Marton et al., 2000; Hudec and Jackson, 2004; Rowan et al., 2014; Brun and Fort, 2004; 2011). This model cannot, however, explain the wide range of patterns and styles of predominantly contraction-related salt structures seen on the mid-slope of the Outer Kwanza Basin, offshore Angola (see section 5). Here, the mid-slope domain is characterized by the synchronous formation of extensional and contractional salt-related structures. Evans and Jackson (2019) invoke spatially complex salt flow over base-salt relief to explain this spatially complex pattern of deformation southeast of the present study area, illustrating the formation, translation, and rotation of RSBs and flanking salt walls. They highlighted the key role played by the seaward-edge of the Flamingo Platform, but did not especially focus on the types and kinematics of contraction-related salt-tectonic structures. We show that local base-salt relief, and not only the Flamingo Platform, control the diversity and evolution of salt-related contractional styles in the mid-slope domain of the Outer Kwanza Basin. Similar relationships are documented in the Santos and Campos Basins, offshore Brazil, and in the Gulf of Mexico (e.g. Dooley et al., 2017; Dooley and Hudec, 2017; Pichel et al., 2019).

Our study illustrates that, in the mid-slope domain of the Outer Kwanza Basin, translation of salt and its overburden across broadly parallel-trending basin margin ramps (i.e. NW and N-trending) causes not only early contraction (i.e. the initiation of salt anticlines when salt is capped by a relatively thin roof), but also relatively later inversion of precursor salt structures (i.e. squeezing and active rise of diapirs). Similar strain patterns are predicted by physical models, which show that salt flow across up-flow- and/or downflow- facing steps along the base-salt generate local contractional and extensional structural styles (Dooley et al., 2017; 2018; Dooley and Hudec, 2017; Ferrer et al., 2017). As such, in mid-slope domain of the Outer Kwanza Basin, translation of salt and its overburden across multiple ramps results in multi-phase shortening and extension. This mechanism explains why contractional structures occur in the mid-slope of the Outer Kwanza Basin, in the midst of an array of extensional structures.

In the mid-slope domain of the Outer Kwanza Basin, the formation of primary salt welds above seaward-facing base-salt ramp is a key control on local squeezing of pre-existing extensional diapirs (walls), which in some cases leads to thrust-related deformation of their roofs. As these salt structures translated seaward, the welds acted as buttresses, generating updip local compressional stress field. In this way, the formation of a primary weld by shear-thinning during regional translation is mechanically comparable to the pinch-out of salt above downslope, base-salt surface as predicted from the physical models of Dooley et al. (2007). The process described here is similar to that in the Northern Gulf of Mexico, where primary welding causes otherwise freely horizontally translating minibasins to collide, inducing the formation of contractional structures (see Duffy et al., 2020; Fernandez et al., 2020). In our study, the updip local compressional stress field replaces the extensional stress field previously located above the seaward-dipping ramp (labelled 2; Fig. 3b).

The formation of contractional structures in the mid-slope domain is more complex due to the combined effect of bulk rotation (i.e. a type of distributed shear) of the salt overburden and pre-existing salt structures. Previous studies using 3D seismic reflection data suggest this rotation may be caused by salt flow across complex base-salt reliefs (i.e. isolated base-salt high and/or convex- and concave-into-the-basin ramps) (Pichel et al., 2019), and/or spatial variations in the original salt thickness (see discussion above; see also Evans and Jackson, 2019). The results of our study are consistent with the latter hypothesis, but we also suggest that a key control on salt structure and overburden rotation is the presence of local base-salt relief (i.e. rotation only occurred in the south of the study area, where base-salt relief was more subdued). The broadly linear ramps and isolated base-salt highs in the north and centre of the study area perturbed seaward flow of salt and its overburden (c.f. isolated base-salt high model of Dooley et al., 2018), resulting in salt flow faster in the south. Concave-ramps in the southwest also served to amplify and rotate contractional structures as they translated seaward (see section 7 and 8) (convergent gliding; Cobbold and Szatmari, 1991).

We argue that using the geometry and evolution of RSBs alone to understand the kinematics of salt-detached yields an incomplete picture (e.g. Pichel et al., 2018; Evan and

Jackson, 2019); such analyses should be supported by the detailed mapping of base-salt relief and overlying salt-tectonic structures. For example, rather than simply being associated with bulk clockwise rotation of the overburden as suggested by Evans and Jackson (2019), we observe that RSBs are locally associated with the local growth of salt-detached strike-slip faults (i.e. a type of focused shear), at least in the northern part of the basin during the Late Miocene to Present (Fig. 11 f, g). The formation of strike-slip faults records spatial differences in the rate and magnitude of the seaward translation of salt and its overburden, with this effect maybe being enhanced in the presence of base-salt relief. For example, where such relief is present, along-strike variations in translation may be relatively sharp, leading to focused shear and strike-slip faulting. Further work is required to establish the detailed geometric and kinematic relationship between salt-detached strike-slip faults and base-salt relief.

10. Conclusion

We used 3D seismic reflection data to examine the structural style, distribution, and kinematics of salt structures in the mid-slope domain of the Outer Kwanza Basin, offshore Angola. We showed that a suite of predominantly contractional salt or salt-related structures, including salt anticlines and squeezed walls, as well as salt-detached thrusts, trend either parallel or oblique to, and are sometimes located directly above, NW-, N-, NE-trending ramps along the base-salt. Some of the structures are separated by apparent primary salt welds.

Using section restorations to identify the pre-translation location of the salt and salt-related structures, we argue that base-salt relief and the formation of primary salt welds controlled the presence and evolution of contractional salt-related structures. We also show that the seaward translation of salt and its overburden began in the Albian, soon after salt deposition, and that the absolute magnitude of translation varied from13-22 km. The interaction between base-salt highs and salt welds, and the seaward-translating salt structures lead to locally intense overprinting of extensional and compressional strain fields. Seaward translation was also associated with bulk clockwise rotation of salt structures and related overburden structures. We suggest that during early translation, this rotation was driven by regional, along-strike changes in salt thickness, with thicker, faster-flowing salt and overburden in the SE and thinner, slower-moving salt and overburden in the NW. However, during later translation, as salt had locally thinned due to the flow of salt into growing diapirs, base-salt relief became relatively more important; i.e. in the north and centre, where base-salt relief was more pronounced, the seaward translation of salt and its overburden translation was more tortuous and overall slower compared to the south.

We demonstrate that detailed mapping of base-salt relief and overlying salt-structures reveal complex structural styles and kinematics of salt-related deformation in the translational domains of salt basins.

Acknowledgement

The authors wish to thank Sian Evans, Leonardo Pichel and Alexander Coleman for discussions during the course of this study. A big thank you to CGG for providing access to the high-quality 3D seismic dataset and for allowing publication of the results of this study. The main author would like to thank the Indonesia Endowment Fund for Education (LPDP) for sponsoring his PhD research. The main author would also like to thank Benyamin Sapiie, Keigo Kitamura, Igna Hadi Suparyanto and Indonesian Institute of Science (LIPI) for indirect assistance and administrative support in his PhD research. The authors also acknowledge Schlumberger for providing Petrel software and Petroleum Expert for provision of a licence for 2D Move software to Imperial College.

References

Brownfield, M. E., and Charpentier, R. R., 2006, Geology and Total Petroleum Systems of the West-Central Coastal Province (7203), West Africa.

Brun, J.-P., and Fort, X., 2004, Compressional salt tectonics (Angolan margin): Tectonophysics, v. 382, no. 3-4, p. 129-150.

Brun, J.-P., and Fort, X., 2011, Salt tectonics at passive margins: Geology versus models: Marine and Petroleum Geology, v. 28, no. 6, p. 1123-1145.

Brun, J.-P., and Mauduit, T. P. O., 2009, Salt rollers: Structure and kinematics from analogue modelling: Marine and Petroleum Geology, v. 26, no. 2, p. 249-258.

Cobbold, P. R., and Szatmari, P., 1991, Radial gravitational gliding on passive margins: Tectonophysics, v. 188, no. 3, p. 249-289.

Cramez, C., and Jackson, M. P. A., 2000, Superposed deformation straddling the continental-oceanic transition in deep-water Angola: Marine and Petroleum Geology, v. 17, no. 10, p. 1095-1109.

Davison, I., Anderson, L., and Nuttall, P., 2012, Salt deposition, loading and gravity drainage in the Campos and Santos salt basins: Geological Society, London, Special Publications, v. 363, no. 1, p. 159-174.

Dooley, T. P., and Hudec, M. R., 2017, The effects of base-salt relief on salt flow and suprasalt deformation patterns — Part 2: Application to the eastern Gulf of Mexico: Interpretation: SEG, v. 5, no. 1.

Dooley, T. P., Hudec, M. R., Carruthers, D., Jackson, M. P. A., and Luo, G., 2017, The effects of base-salt relief on salt flow and suprasalt deformation patterns — Part 1: Flow across simple steps in the base of salt: Interpretation: SEG, v. 5, no. 1.

Dooley, T. P., Hudec, M. R., Pichel, L. M., and Jackson, M. P. A., 2018, The impact of base-salt relief on salt flow and suprasalt deformation patterns at the autochthonous, paraautochthonous and allochthonous level: insights from physical models: Geological Society, London, Special Publications, v. 476, p. SP476.413.

Dooley, T. P., Jackson, M. P. A., and Hudec, M. R., 2007, Initiation and growth of salt-based thrust belts on passive margins: results from physical models: Basin Research, v. 19, no. 1, p. 165-177.

Dooley, T. P., Jackson, M. P. A., and Hudec, M. R., 2009, Inflation and deflation of deeply buried salt stocks during lateral shortening: Journal of Structural Geology, v. 31, no. 6, p. 582-600.

Duffy, O. B., Fernandez, N., Peel, F. J., Hudec, M. R., Dooley, T. P., and Jackson, C. A. L., 2020, Obstructed minibasins on a salt-detached slope: An example from above the Sigsbee canopy, northern Gulf of Mexico: Basin Research, v. 32, no. 3, p. 505-524.

Duval, B., Cramez, C., and Jackson, M. P. A., 1992, Raft tectonics in the Kwanza Basin, Angola: Marine and Petroleum Geology, v. 9, no. 4, p. 389-404.

Erdi, A., and Jackson, C. A. L., 2020, Base-salt Relief Controls Salt-related Contractional Styles in the Translational Domain of the Outer Kwanza Basin, offshore Angola, EGU General Assembly: Online.

Evans, S. L., and Jackson, C. A. L., 2019, Base-salt relief controls salt-related deformation in the Outer Kwanza Basin, offshore Angola: Basin Research, v. 0, no. 0.

Fernandez, N., Duffy, O. B., Peel, F., and Hudec, M. R., 2020, Influence of minibasin obstruction on canopy dynamics in the northern Gulf of Mexico: Basin Research, v. n/a, no. n/a.

Ferrer, O., Gratacós, O., Roca, E., and Muñoz, J., 2017, Modeling the interaction between presalt seamounts and gravitational failure in salt-bearing passive margins: The Messinian case in the northwestern Mediterranean Basin, v. 5, p. SD115-SD133.

Fort, X., Brun, J.-P., and Chauvel, F., 2004, Salt tectonics on the Angolan margin, synsedimentary deformation processes: AAPG Bulletin, v. 88, no. 11, p. 1523-1544.

Gaullier, V., Brun, J. P., Guerin, G., and Lecanu, H., 1993, Raft Tectonics - the Effects of Residual Topography Below a Salt Decollement: Tectonophysics, v. 228, no. 3-4, p. 363-381.

Guiraud, M., Buta-Neto, A., and Quesne, D., 2010, Segmentation and differential post-rift uplift at the Angola margin as recorded by the transform-rifted Benguela and oblique-to-orthogonal-rifted Kwanza basins: Marine and Petroleum Geology, v. 27, no. 5, p. 1040-1068.

Hudec, M. R., and Jackson, M. P. A., 2002, Structural segmentation, inversion, and salt tectonics on a passive margin: Evolution of the Inner Kwanza Basin, Angola: GSA Bulletin, v. 114, no. 10, p. 1222-1244.

Hudec, M. R., and Jackson, M. P. A., 2004, Regional restoration across the Kwanza Basin, Angola: Salt tectonics triggered by repeated uplift of a metastable passive margin: AAPG Bulletin, v. 88, no. 7, p. 971-990.

Jackson, C. A. L., Jackson, M. P. A., and Hudec, M. R., 2015, Understanding the kinematics of salt-bearing passive margins: A critical test of competing hypotheses for the origin of the Albian Gap, Santos Basin, offshore Brazil: Geological Society of America Bulletin, v. 127, no. 11-12, p. 1730-1751.

Jackson, M. P. A., and Hudec, M. R., 2005, Stratigraphic record of translation down ramps in a passive-margin salt detachment: Journal of Structural Geology, v. 27, no. 5, p. 889-911.

Jackson, M. P. A., and Hudec, M. R., 2009, Interplay of Basement Tectonics, Salt Tectonics, and Sedimentation in the Kwanza Basin, Angola, AAPG International Conference and Exhibition: Cape Town, South Africa.

Jackson, M. P. A., and Hudec, M. R., 2017, Salt Tectonics: Principles and Practice, Cambridge, Cambridge University Press.

Jackson, M. P. A., Hudec, M. R., Jennette, D. C., and Kilby, R. E., 2008, Evolution of the Cretaceous Astrid thrust belt in the ultradeep-water Lower Congo Basin, Gabon: Aapg Bulletin, v. 92, no. 4, p. 487-511.

Karner, G. D., and Driscoll, N. W., 1999, Tectonic and stratigraphic development of the West African and eastern Brazilian Margins: insights from quantitative basin modelling.

Karner, G. D., Driscoll, N. W., and Barker, D. H. N., 2003, Syn-rift regional subsidence across the West African continental margin: the role of lower plate ductile extension.

Lundin, E. R., 1992, Thin-skinned extensional tectonics on a salt detachment, northern Kwanza Basin, Angola: Marine and Petroleum Geology, v. 9, no. 4, p. 405-411.

Marton, L. G., Tari GáBor, C., and Lehmann Christoph, T., 2000, Evolution of the Angolan Passive Margin, West Africa, With Emphasis on Post-Salt Structural Styles: Atlantic Rifts and Continental Margins.

Moulin, M., Aslanian, D., Olivet, J.-L., Contrucci, I., Matias, L., G´eli, L., Klingelhoefer, F., Nouz´e, H., R´ehault, J.-P., and Unternehr, P., 2005, Geological constraints on the evolution of the Angolan margin based on reflection and refraction seismic data (ZaïAngo project): Geophysical Journal International, v. 162, no. 3, p. 793–810.

Peel, F. J., 2014, The engines of gravity-driven movement on passive margins: Quantifying the relative contribution of spreading vs. gravity sliding mechanisms: Tectonophysics, v. 633, p. 126-142.

Pichel, L. M., Jackson, C. A. L., Peel, F., and Dooley, T. P., 2019b, Base-salt relief controls salt-tectonic structural style, São Paulo Plateau, Santos Basin, Brazil: Basin Research, v. 0, no. 0.

Pichel, L. M., Peel, F., Jackson, C. A. L., and Huuse, M., 2018a, Geometry and kinematics of salt-detached ramp syncline basins: Journal of Structural Geology, v. 115, p. 208-230.

Quirk, D. G., Schødt, N., Lassen, B., Ings, S. J., Hsu, D., Hirsch, K. K., and Von Nicolai, C., 2012, Salt tectonics on passive margins: examples from Santos, Campos and Kwanza basins: Geological Society, London, Special Publications, v. 363, no. 1, p. 207-244.

Rowan, M., Peel, F., and Vendeville, B., 2004, Gravity-driven Fold Belts on Passive Margins, *in* McClay, K. R., ed., Thrust Tectonics and Hydrocarbon Systems, Volume 82, AAPG Memoir, p. 157-182.

Rowan, M. G., Jackson, M. P. A., and Trudgill, B. D., 1999, Salt-related fault families and fault welds in the northern Gulf of Mexico: AAPG Bulletin-American Association of Petroleum Geologists, v. 83, no. 9, p. 1454-1484.

Rowan, M. G., and Ratliff, R. A., 2012, Cross-section restoration of salt-related deformation: Best practices and potential pitfalls: Journal of Structural Geology, v. 41, p. 24-37.

Serié, C., Huuse, M., Schødt Niels, H., Brooks James, M., and Williams, A., 2015, Subsurface fluid flow in the deep-water Kwanza Basin, offshore Angola: Basin Research, v. 29, no. 2, p. 149-179.

Valle, P. J., Gjelberg, J.G., and Helland-Hansen, W., 2001, Tectonostratigraphic development in the eastern Lower Congo Basin, offshore Angola, West Africa: Marine and Petroleum Geology, v. 18, no. 8, p.909-927.

Vendeville, B. C., and Jackson, M. P. A., 1992a, The Fall of Diapirs during Thin-Skinned Extension: Marine and Petroleum Geology, v. 9, no. 4, p. 354-371.

Vendeville, B. C., and Jackson, M. P. A., 1992b, The rise of diapirs during thin-skinned extension: Marine and Petroleum Geology, v. 9, no. 4, p. 331-354.

Vendeville, B. C., and Nilsen, K. T., 1993, Episodic Growth of Salt Diapirs Driven By Horizontal Shortening, *in* Adam's Mark, H., ed., Salt, Sediment and Hydrocarbons, SEPM Society for Sedimentary Geology.

Von Nicolai, C., 2011, The Interplay of Salt Movements and Regional Tectonics at the Passive Continental Margin of the South Atlantic, Kwanza Basin.

Wagner, B. H., and Jackson, M. P. A., 2011, Viscous flow during salt welding: Tectonophysics, v. 510, no. 3, p. 309-326.

Tables Captions

Table 1: Horizon interpretation and comparative interpretation from previous publications.

Table 2: Salt structure inventory tabulating salt structures characteristic in the study area. Seismic data courtesy of CGG Multi-Client.

Table 3: Supra-salt structural style Inventory tabulating supra-salt fault characteristic in the study area. Seismic data courtesy of CGG Multi-Client.

Figures Captions

Figure 1: a) Simplified regional structural map of offshore Angola, (b) Regional section across offshore Angola (modified from Hudec and Jackson, 2002; Hudec and Jackson, 2004; Moulin et al., 2005; Jackson and Hudec, 2005; Guiraud et al., 2010; Serie et al., 2015; Erdi and Jackson, 2020).

Figure 2: Simplified regional tectonostratigraphic of offshore Angola (adapted from Hudec and Jackson, 20014; Evan and Jackson, 2019).

Figure 3: Idealized profile of salt flow across base-salt surfaces, resulting in various local salt-related deformations. a) During early stages, salt flow across base-salt step is retarded, inducing contraction and salt thickening. (redrawn from Dooley et al., 2017;2018); b) Late stage evolution of salt flow across a base-salt high block: (1) Increasing salt flow velocity of thickened salt above base-salt high through time induce extension on overburden; (2) Above downdip ramp, rapid extension occurs due to salt flow acceleration; (3) At the base of the ramp, contractional strains occur due to presence of slower-moving salt. (redrawn from Jackson and Hudec., 2017; Dooley et al., 2017;2018); c) During early stage, polyharmonic, salt anticlines are formed due to resultant mechanic between contraction and salt thickening, associated with the salt flow acceleration across a base-salt step, and thicken overburden.

Figure 4: (a) Depth-structure map (left) and interpretative sketch (right) of base salt horizon illustrating base-salt relief and complex ramp (highlighted by red colour) geometries of the Flamingo platform and surroundings. (b) Depth thickness map (left) and interpretative sketch (right) of Aptian salt illustrating morphology and salt structures distribution. (c) Depth-structure map (left) and interpretative sketch (right) of the top Albian seismic horizon illustrating fault framework on overburden.

Figure 5: Strike-oriented seismic profile illustrating salt-related structural styles. (a) NW-SE-to-NE-SW cross-section showing salt-related deformations above several local structural highs and ramps. This seismic profile intersects typical triangular profile of reactive piercement salt walls, where inward-dipping salt-detached normal faults are observed at their crest. The strike-slip faults are located above upper tips of base-salt high block, which its dipping either consistent or against dipping ramps. The outer-arc extension faults are associated with turtle anticlines above structural high. b) NW-SE cross-section showing polyharmonic, salt anticlines broadly above relatively flat base-salt surfaces. c) Zoom in on NW-SE cross-section showing polyharmonic, salt anticlines above downdip, SE-dipping ramp. Note the intra-Albian growth strata developed, while shortening strata on the inner arc and thicken salt are observed above upper tips of ramps. d) NW-SE cross-section showing strike-slip fault against dipping ramp, outer-arc bending normal faults over the roof of the squeezed salt anticlines, and relic horn at the crest of the complexed salt walls. Seismic data courtesy of CGG Multi-Client.

Figure 6: Dip-oriented seismic profile illustrating salt-related contractional structural style in the north area. (a) NE-SW cross-section showing salt anticlines with and without associated salt-detached normal and thrust faults are developed above either seaward (SW) or landward (LW)-facing ramp. The SC4 is overlaid by thinned Eocene and tabular Oligocene strata, while the SC5 and the SC6 are overlaid by tabular Eocene and thinned Oligocene strata, implying the salt anticlines grew younger toward NE. (b) NE-SW cross section showing salt anticline are overlaid by intra-Albian growth strata southwestward and progressively older landward, Eocene growth strata. Further northeast, the complex salt walls with associated thrust fault developed above the flat located immediately downdip of the NW-trending, SW-facing ramps, while outer-arc extensional fault developed on its flank. This salt wall is overlaid by RSBs and drape fold on overburden. (c) NE-SW cross section showing outer-arc bending normal faults over the roof of a squeezed salt anticline. Further northeast, a squeezed salt wall is located at the base of the ramp overlying by series of RSBs. The RSBs reflect seaward translation of salt and its overburden. Seismic data courtesy of CGG Multi-Client.

Figure 7: Dip-oriented seismic profile illustrating salt-related contractional structural style in the centre. (a) NE-SW cross section showing diapir fall above complex salt wall in the center, while the complex salt walls with associated NE and SW-dipping thrust faults developed above downdip of the NW-trending, SW-dipping ramp. (b) NE-SW cross section showing polyharmonic, salt anticline in the south west, while in the centre the complex salt wall are presented. Further northeast, RSBs are developed above downdip, seaward-dipping of Flamingo platform. (c) NE-SW cross section showing the complex salt wall in the centre above downdip, seaward-dipping of local structural high. Seismic data courtesy of CGG Multi-Client.

Figure 8: (a) An overlaid base-salt structure with thickness map. (b) An overlaid base-salt structure map with Albian depth structure map.

Figure 9: Restoration of dip-oriented seismic profile illustrating evolution of contractional structural styles in the Outer Kwanza Basin. (a) Restoration of NW-SE seismic profile in the south above structural-high of Y; (b) Restoration of NW-SE seismic profile in the centre above structural-high of W; (c) Restoration of NW-SE seismic profile in the north above structural-high of V.

Figure 10: Graph showing cumulative translation in each of selective cross sections through time (Fig 9). The graph is compared with cumulative rotation of Evan and Jackson (2019).

Figure 11: Map view of salt-related structural evolution using restoration position of three cross sections and RSBs restoration.

Figure 12: Physical model of Dooley et al (2018) simulating effects of local base-salt highs (white boxes) (c.f. Fig 4a; V, W, X, Y and Z) have in three-dimension on: (a) salt-related deformations (b) salt flow seaward in the salt-bearing passive margin. (a) Overhead views of models show rotation at the proximal edge (20-36) and front edge (up to 67^{o}) of the local base-salt highs. (b) the local base-salt high act as salt flow perturbation, resulting in salt flow channelization (i.e. convergent and divergent flow). For full model design in details, see Dooley et al. (2018).

Table

Table 1

Age	Horizon		
	This study	Previous publication	
Late Miocene	Top of Miocene	Top of Miocene	Hudec and Jackson (2004)
		Mi	Serie et al (2015)
Middle Miocene	M2		
Early Miocene	M1		
Oligocene	Oligocene	Og	Serie et al (2015)
		Top Oligocene	Hudec and Jackson (2004)
		O2	Valle et al (2001)
Eocene	Eocene	Eo	Serie et al (2015)
		E1	Valle et al (2001)
Albian	Albian	Alb	Serie et al (2015)
Late Aptian	Salt		
Middle Aptian	Base salt		

Table 2

Map and text name	Example	Geometries: Diagnostic description	Geometries: Orientation: Trend	Geometries: Orientation: Ramp trend association	Geometries: Dimension: Long (m)	Geometries: Dimension: Width (m)	Geometries: Dimension: Height (m)	Geometries: Fault association	Genetic Interpretation: Driving Forces: Initiation	Genetic Interpretation: Driving Forces: Evolution	Genetic Interpretation: Salt-related deformation: Initiation	Genetic Interpretation: Salt-related deformation: Evolution
Salt anticline	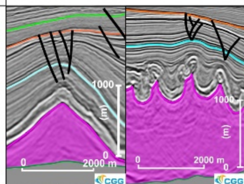	◦Low amplitude, long wavelengths of rounded salt upwelling, concordant contact with overburden ◦Locally, polyharmonic ,high amplitude, short wavelength of rounded salt upwelling ◦In map view, it is laterally either merged into salt walls or gradually died out	NW and N NW, N and NE	Trend broadly parallel to NW-or N-trending ramps; located above updip either landward-or basinward-facing ramps Trend oblique to NW-trending, and parallel to N-trending ramps; broadly located above relatively flat relief	at least 2800	at least 500	up to 2000	◦ Locally dissected by NW-trending symmetric outer-arc extension faults over the roof ◦ Locally dissected by NW, N-trending, landward -dipping thrust faults above the crest, or NW, N-trending, basinward-dipping salt-detached normal faults on the fold limb	Local contraction due to deceleration of salt flow associated with differences in salt thickness between above and base of base -salt high blocks local contraction associated with salt thickness between above and base of base-salt high blocks whilst overburden thicken	Local extensions are located: (i) the upper tip of basinward-facing ramps due to differences in salt thickness (ii) above base-salt high blocks due to increasing of salt-velocity flow	Salt anticlines, with or without thrust faults	Reactive salt walls, salt anticlines dissected by salt-detached normal faults
Squeezed salt anticline	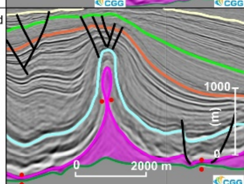	◦Triangular salt pedes tal, secondary salt weld, bulb-shaped head ◦ In map view, it is intersected by either salt-detached normal faults or strike-slip faults	NW	Trend parallel to NW-trending ramps; located above upper-tip of basinward-facing ramps	3500-11000	up to 3000 on salt pedestal	up to 1100	◦ Locally dissected by NW-trending symmetric outer-arc extension faults over the roof	Local contraction due to deceleration of salt flow associated with differences in salt thickness between above and base of base-salt high blocks	◦ Local contraction due to salt flow encounter slower-moving salt on the base of base-salt high block	Salt anticlines	Squeezed salt anticlines
Salt wall and roller	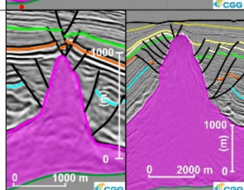	◦Symmetric and asymmetric triangular salt wall, pointed diapir crest ◦Locally, relic horn above the crest ◦Locally, arched roof, rounded diapir crest ◦In map view, it is laterally either died out or merge into other types of salt-related deformations	NW, N and NE	Trend broadly parallel to NW, N and NE-trending, with locally oblique to NW-trending ramps; located broadly above downdip of basinward-facing ramps and locally above relatively flat relief	4000-75000	1100-4270	up to 3000	NW, N, NE-trending, inward-dipping, locally rotated, salt-detached normal faults on the flank and over the crest.	◦ Local extension due to increasing of salt-velocity flow above base-salt high blocks ◦ Local extension above the upper tip of basinward-facing ramps due to different salt thickness	◦ Local extension due to salt flow to another part of salt wall ◦ Local contraction due to salt flow encounter slower-moving salt at the base of base-salt high block	Reactive salt wall	Diapir fall Active piercement (Active rise)
Squeezed salt wall and roller	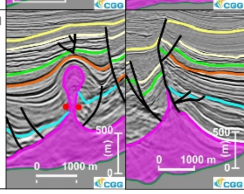	◦Triangular salt pedestal, locally secondary salt weld and bulb-shaped head ◦In map view, it is laterally merged into a reactive salt wall, intersected by strike-slip faults, or gradually died out	NW	Parallel to NW-trending ramps; broadly located above downdip of basinward-facing ramps, and locally located above relatively flat relief	at least 5000	at least 1800	up to 1900	◦ NW, N, NE-trending, inward-dipping, salt-detached normal faults on the flank or the triangular pedestal ◦ Locally, NW-trending, basinward, landward-dipping thrust fault over the crest ◦ Locally, outer arc-extension faults over the roof	◦ Local extension due to increasing of salt velocity above base-salt high blocks ◦ Local extension above the upper tip of basinward-facing ramps due to different salt thickness	◦ Local contraction due to salt flow encounter slower-moving salt at the base of base-salt high block ◦ Local contraction due to salt flow encountering salt weld, which acts as a buttress	Reactive salt wall	Squeezed salt wall and roller

Table 3

Map and text code	Example	Geometries						Maximum throw (m)	Offset	Stratigraphic Association	Genetic
		Diagnostic description	Orientation			Dimension					
			Strike	Dipping	Ramp trend association	Long (m)	Dip (°)				
Salt-detached normal fault	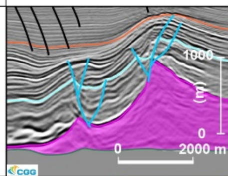	◦Planar to locally rotated normal and listric growth fault that sole into salt layer ◦In map view, it forms arcuate-to-planar array faults which are laterally die out into salt structures	NW, N and NE	Locally inward -dipping toward salt walls; dominantly basinward and landward	Strike broadly parallel to NW, N, NE-trending, and locally oblique to NW-trending ramps; located either above relatively flat relief or downdip of basinward-facing ramps	at least 2500	56°-86°	up to 500	◦ Normal offset at Albian-Eocene strata, and locally at Albian-Holocene; fault tip die out downward into the salt layer, and upward into overburden	◦ Generally, Eocene strata thicken toward fault planes. ◦ Locally, Albian, Oligocene-Holocene strata thicken toward fault plane located between isolated structural high and Flamingo platform ◦ Locally, Oligocene and Middle Miocene strata thicken toward fault plane associated with the active rise of SW2 in the centre. ◦ Locally, Early Miocene and Late Miocene strata thicken associated with diapir fall	◦ Local extension due to increasing of salt velocity above base-salt high block ◦ Local extension above basinward-facing ramp due to different salt thickness
Outer-arc extensional fault	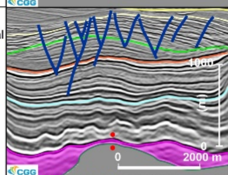	◦Planar normal faults forms symmetric-to-asymmetric graben, developing either on the hanging zone of the anticline or axial trace of the monocline ◦In map view,it forms curved-to-planar patterns, parallel to the underlying fold	NW and NE	Inward-dipping toward fold hinge zone; locally antithetic to salt-detached normal fault	Strike broadly parallel to underlying NW- or NE-trending ramps; located above relatively flat relief, local structural high or downdip of basinward-facing ramps	at least 2000	70°	up to 100	◦ Planar normal offsets between Albian and Middle Miocene strata depend on salt-related structures; fault tip die out both upward and downward into overburden	◦ Relatively, lack associated growth strata toward fault planes	◦ Outer arc bending due to folded strata related to: (i) extension associated with bending of rollover monocline, located on the hanging wall of salt-detached normal fault; (ii) contraction of salt anticlines.
Strike-slip fault	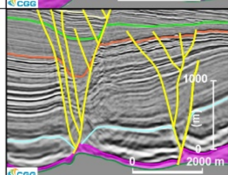	◦Planar normal growth fault, locally form negative flower structure, and partial coupling with base-salt ◦In map view,it forms planar patterns, indicating lateral displacement over salt structures,salt-detached normal fault and thrust fault	NE	Southeast and northwest	Strike parallel to NE-trending ramps; located either above relatively flat relief, or downdip of SE-or NW-facing ramps	at least 10000	62°-87°	up to 800 on dip-slip; up to 3000 on strike-slip	◦ Planar normal offsets between Albian, and Oligocene-Holocene strata; fault tip die out downward into salt layer and die out upward into overburden	◦ Albian strata broadly tabular toward fault plane ◦ Locally, Eocene-Oligocene strata, and Late Miocene-Holocene strata thicken toward fault plane	◦ Different translation rate due to different salt thickness associated with base-salt relief oriented parallel to salt flow
Thrust fault	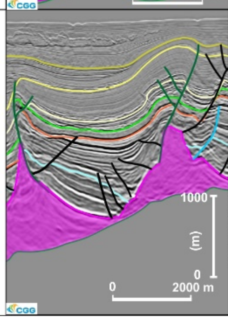	◦Planar thrust fault that sole into the crest of salt structures. Locally, antithetic extensional faults, inverted wedge and growth fold are presented in the hanging wall of the fault ◦In map view, it forms planar-to-arcuate pattern, which laterally either merges into salt-detached normal fault or dies out into salt walls	NW	Landward	Strike parallel to NW- or N-trending ramps; located above downdip of landward-facing ramps	at least 10000	45°-70°	up to 100	◦ Reverse offset at Albian strata; fault tip die out downward to the crest of salt-cored anticlines and upward into Eocene strata	◦ Intra-Oligocene strata onlap onto growth fold associated with thrust faults	◦ Local contraction is due to decelerations of salt flow associated with differences of salt thickness between above and base of base-salt high block.
					Strike parallel to NW-trending ramps; located above downdip of basinward-facing ramps			up to 500	◦ Locally, reverse offset at Eocene-Middle Miocene strata; fault tip die out downward into the crest of salt walls , and upward into Late Miocene strata	◦ Eocene strata thicken toward fault planes ◦ Oligocene-Early Miocene strata broadly tabular toward fault planes ◦ Inverted wedge on Middle Miocene strata ◦ Intra-Late Miocene strata onlap onto hanging wall of fault planes	◦ Local contraction is due to salt flow encounter salt weld, which acts as a buttress
				Basinward				up to 200	◦ Reverse offset at Eocene-Middle Miocene strata; fault tip die out downward to the crest of salt walls, and upward into Late Miocene strata	◦ Locally, Eocene strata thicken toward fault planes ◦ Locally, Oligocene strata broadly tabular toward fault planes ◦ Locally, inverted wedge on Early Miocene-Holocene strata ◦ Late Miocene strata onlap onto inverted wedge and truncated	◦ Local contraction is due to salt flow encounter slower-moving salt at the base of base-salt high block

Figures

Figure 1

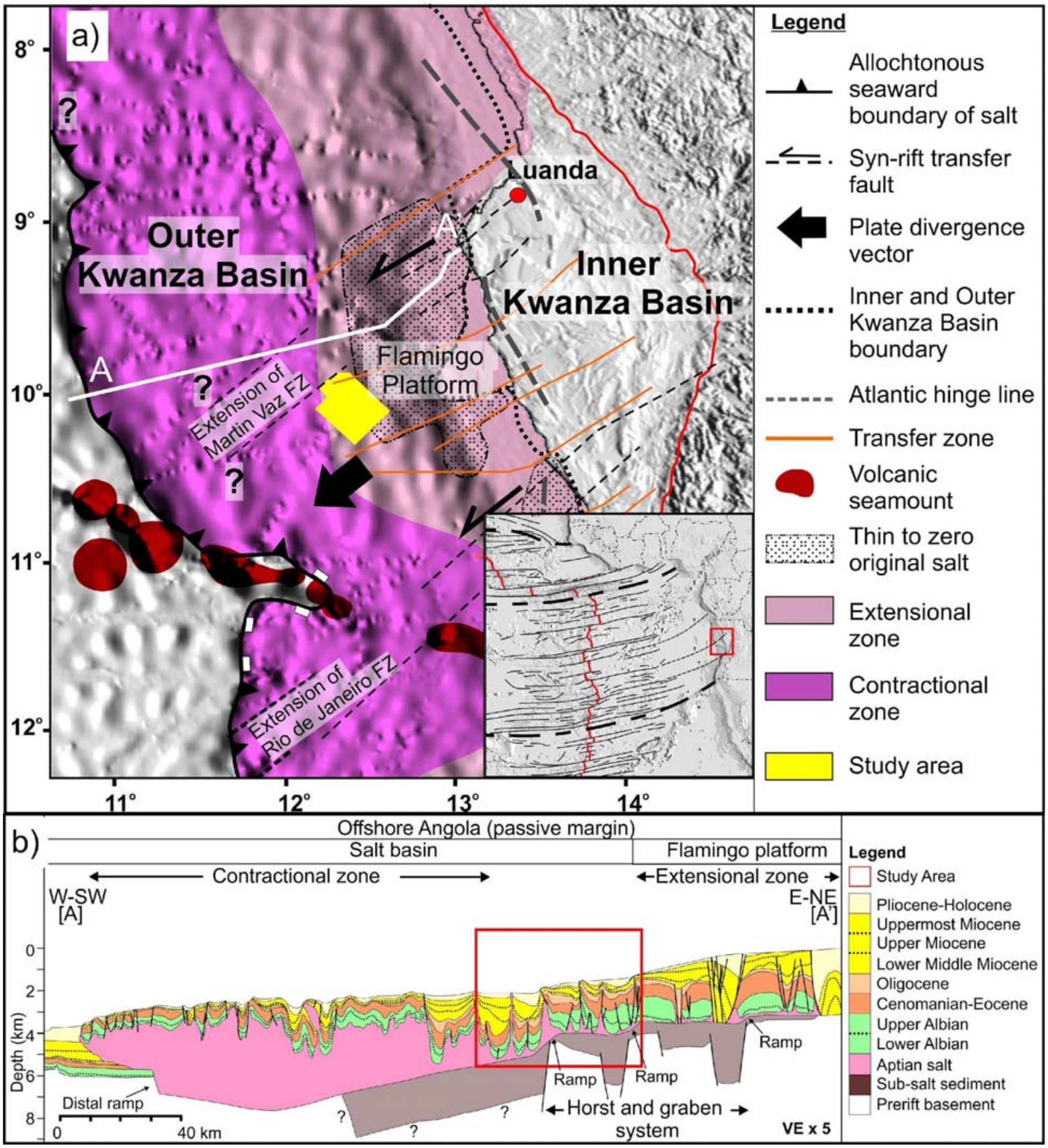

Figure 2

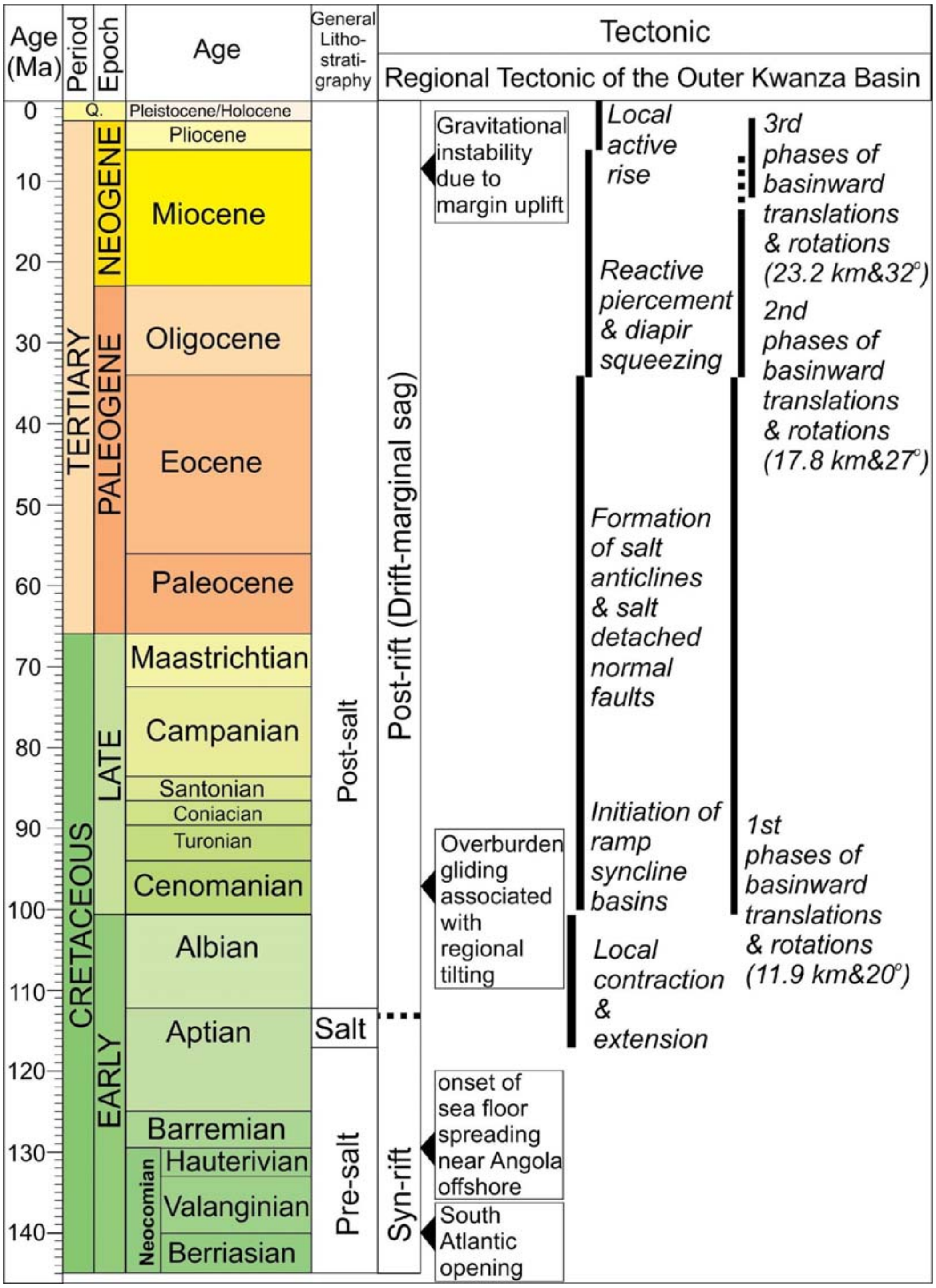

Age (Ma)
Period
Epoch
Age
General Litho-strati-graphy
Tectonic
Regional Tectonic of the Outer Kwanza Basin
0
10
20
30
40
50
60
70
80
90
100
110
120
130
140
Q.
TERTIARY
CRETACEOUS
NEOGENE
PALEOGENE
LATE
EARLY
Neocomian
Pleistocene/Holocene
Pliocene
Miocene
Oligocene
Eocene
Paleocene
Maastrichtian
Campanian
Santonian
Coniacian
Turonian
Cenomanian
Albian
Aptian
Barremian
Hauterivian
Valanginian
Berriasian
Post-salt
Salt
Pre-salt
Post-rift (Drift-marginal sag)
Syn-rift
Gravitational instability due to margin uplift
Overburden gliding associated with regional tilting
onset of sea floor spreading near Angola offshore
South Atlantic opening
Local active rise
Reactive piercement & diapir squeezing
Formation of salt anticlines & salt detached normal faults
Initiation of ramp syncline basins
Local contraction & extension
3rd phases of basinward translations & rotations (23.2 km&32°)
2nd phases of basinward translations & rotations (17.8 km&27°)
1st phases of basinward translations & rotations (11.9 km&20°)

Figure 3

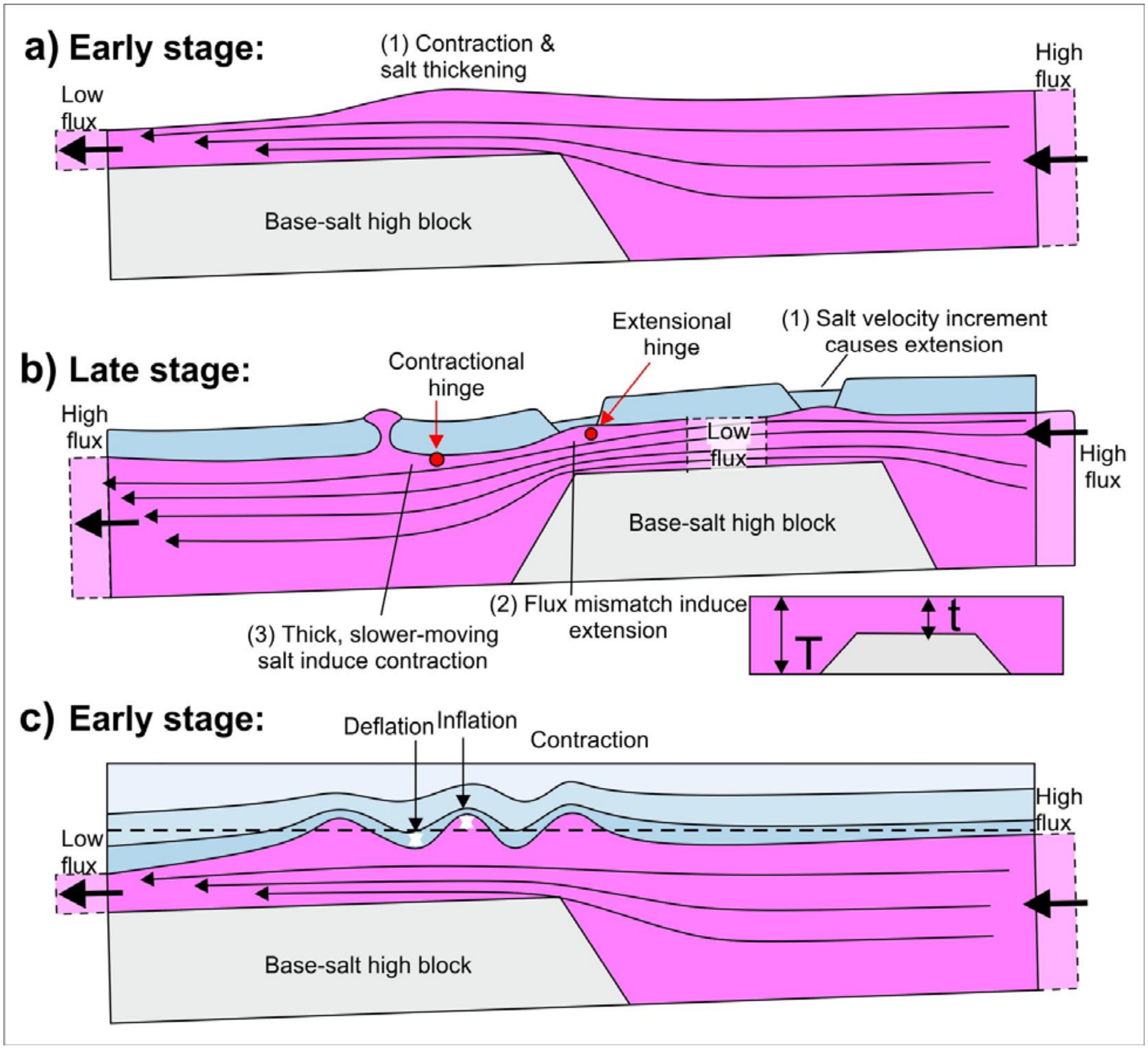
a) Early stage:
(1) Contraction & salt thickening
Low flux
High flux
Base-salt high block
b) Late stage:
Contractional hinge
Extensional hinge
(1) Salt velocity increment causes extension
High flux
Low flux
High flux
Base-salt high block
(2) Flux mismatch induce extension
(3) Thick, slower-moving salt induce contraction
T
t
c) Early stage:
Deflation
Inflation
Contraction
Low flux
High flux
Base-salt high block

Figure 4

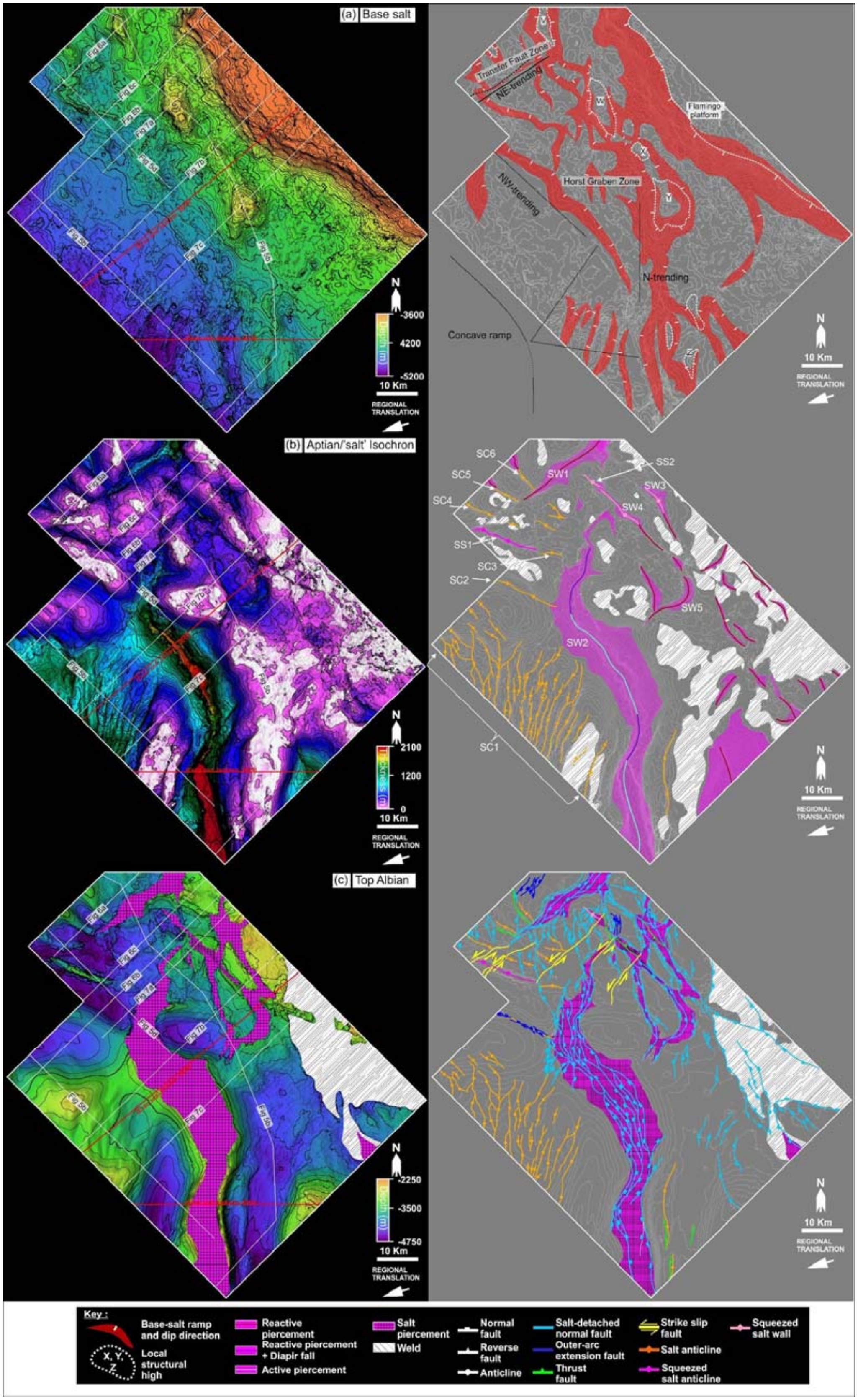

(a) Base salt
Transfer Fault Zone
NE-trending
Flamingo platform
Horst Graben Zone
NW-trending
N-trending
Concave ramp
Depth (m)
-3600
4200
-5200
10 Km
REGIONAL TRANSLATION
(b) Aptian/'salt' Isochron
SC6
SC5
SC4
SS1
SC3
SC2
SC1
SW1
SS2
SW3
SW4
SW5
SW2
2100
1200
0
(c) Top Albian
-2250
-3500
-4750
Key :
Base-salt ramp and dip direction
X, Y, Z
Local structural high
Reactive piercement
Reactive piercement + Diapir fall
Active piercement
Salt piercement
Weld
Normal fault
Reverse fault
Anticline
Salt-detached normal fault
Outer-arc extension fault
Thrust fault
Strike slip fault
Salt anticline
Squeezed salt anticline
Squeezed salt wall

Figure 5

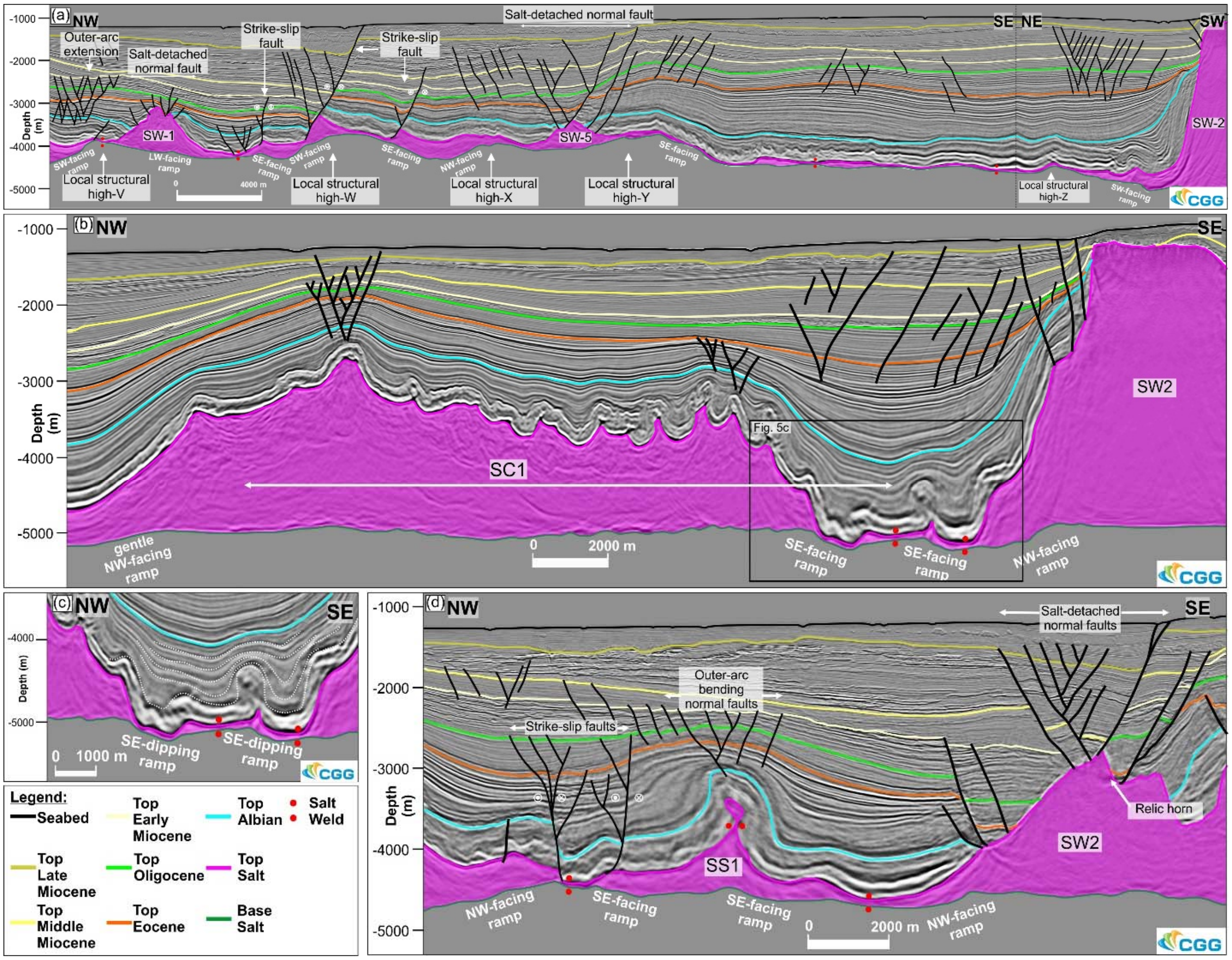

(a)
NW
Outer-arc extension
Salt-detached normal fault
Strike-slip fault
Strike-slip fault
Salt-detached normal fault
SE
NE
SW
SW-1
SW-5
SW-2
Depth (m)
-1000
-2000
-3000
-4000
-5000
SW-facing ramp
LW-facing ramp
SE-facing ramp
SW-facing ramp
SE-facing ramp
NW-facing ramp
SE-facing ramp
SW-facing ramp
Local structural high-V
Local structural high-W
Local structural high-X
Local structural high-Y
Local structural high-Z
0
4000 m
CGG
(b)
NW
SE
SC1
SW2
Fig. 5c
gentle NW-facing ramp
SE-facing ramp
SE-facing ramp
NW-facing ramp
0
2000 m
CGG
(c)
NW
SE
-4000
-5000
Depth (m)
SE-dipping ramp
SE-dipping ramp
0
1000 m
CGG
Legend:
Seabed
Top Early Miocene
Top Albian
Salt Weld
Top Late Miocene
Top Oligocene
Top Salt
Top Middle Miocene
Top Eocene
Base Salt
(d)
NW
SE
Salt-detached normal faults
Outer-arc bending normal faults
Strike-slip faults
Relic horn
SS1
SW2
NW-facing ramp
SE-facing ramp
SE-facing ramp
NW-facing ramp
0
2000 m
CGG

Figure 6

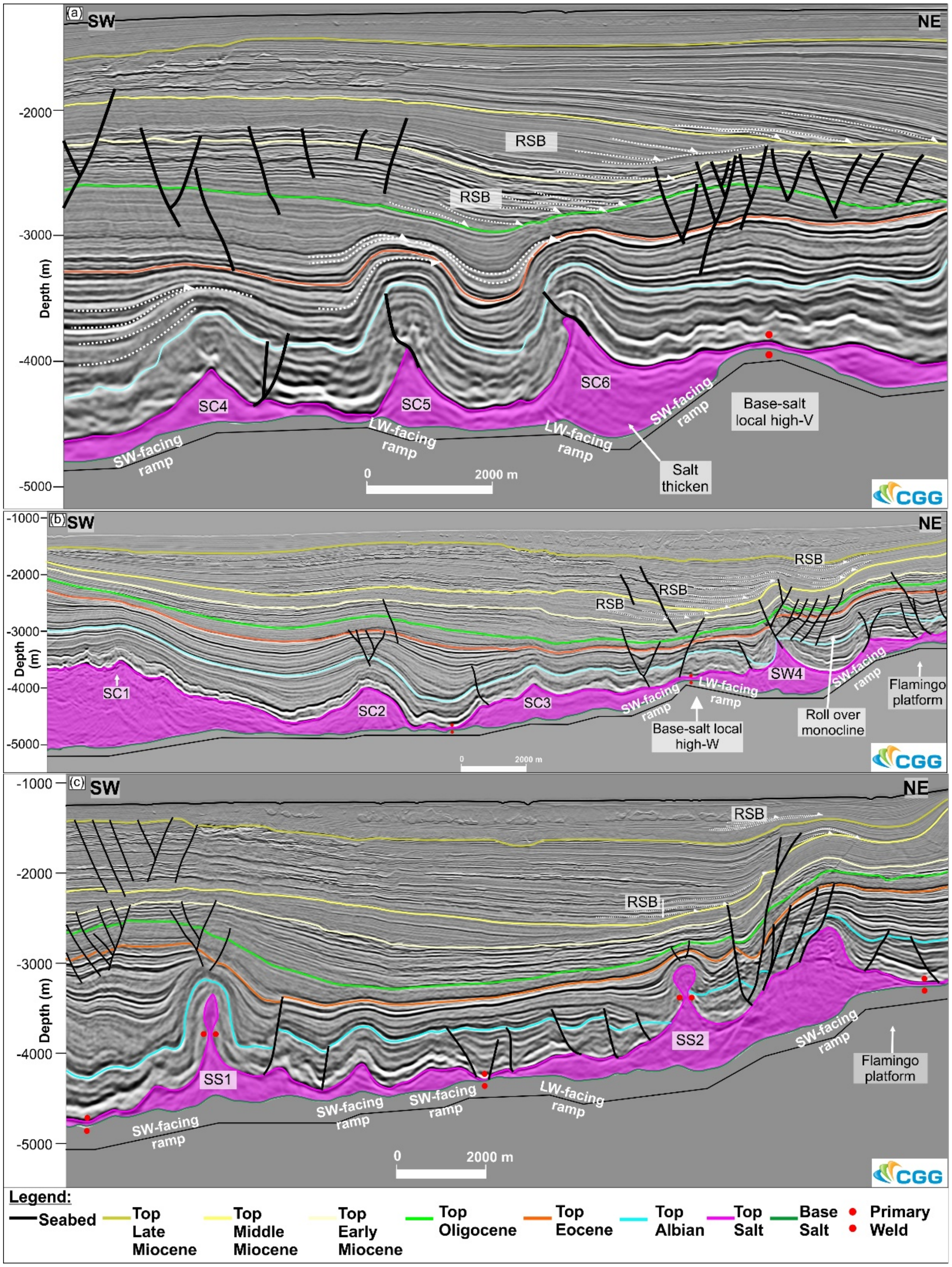
(a) SW
NE
-2000
-3000
-4000
-5000
Depth (m)
RSB
RSB
SC4
SC5
SC6
SW-facing ramp
LW-facing ramp
LW-facing ramp
SW-facing ramp
Base-salt local high-V
Salt thicken
0 2000 m
CGG
(b) SW
NE
-1000
-2000
-3000
-4000
-5000
Depth (m)
RSB
RSB
RSB
SC1
SC2
SC3
SW4
SW-facing ramp
LW-facing ramp
SW-facing ramp
Base-salt local high-W
Roll over monocline
Flamingo platform
CGG
(c) SW
NE
-1000
-2000
-3000
-4000
-5000
Depth (m)
RSB
RSB
SS1
SS2
SW-facing ramp
SW-facing ramp
SW-facing ramp
LW-facing ramp
SW-facing ramp
Flamingo platform
0 2000 m
CGG
Legend:
Seabed
Top Late Miocene
Top Middle Miocene
Top Early Miocene
Top Oligocene
Top Eocene
Top Albian
Top Salt
Base Salt
Primary Weld

Figure 7

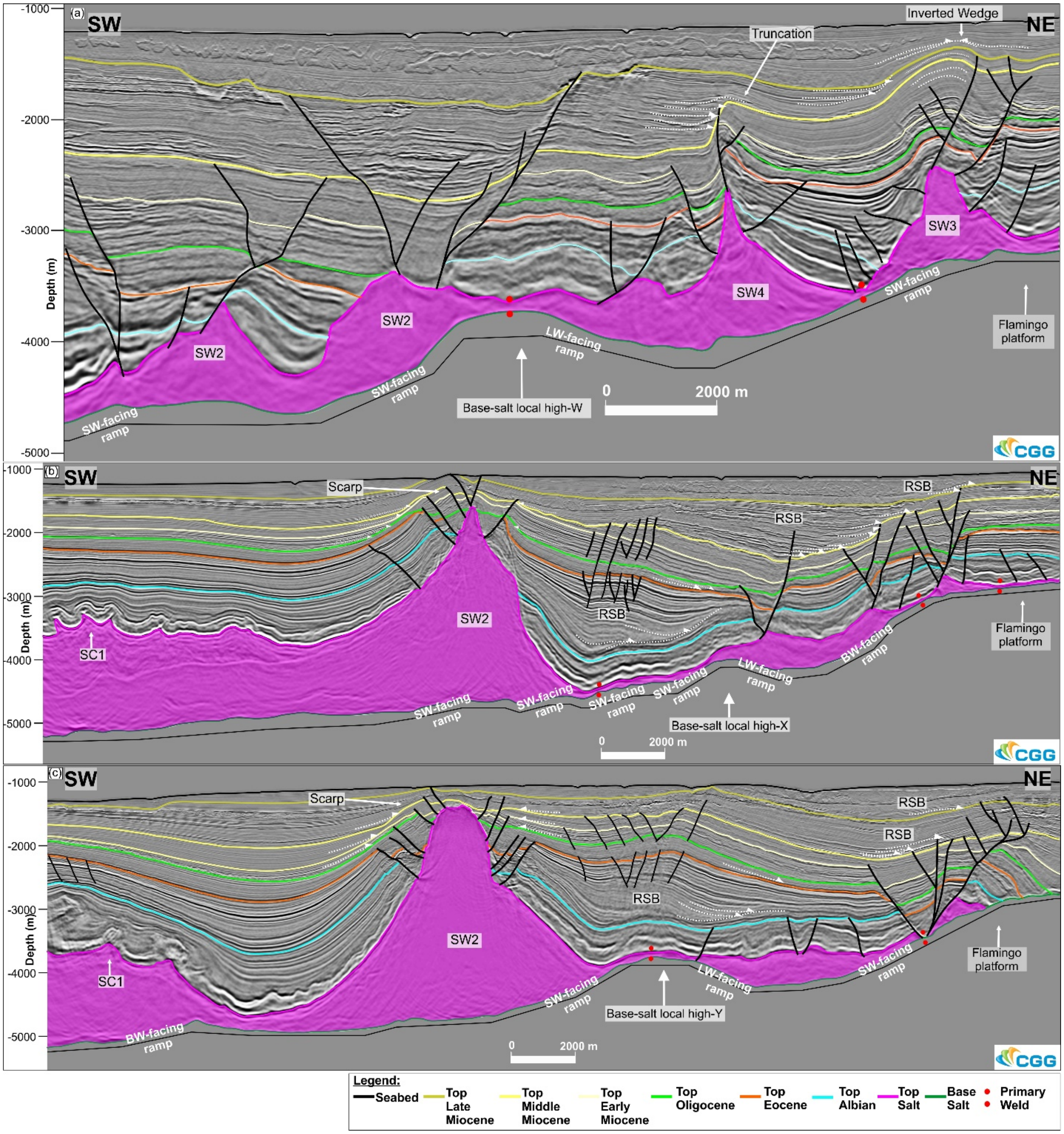
(a)
SW
NE
Inverted Wedge
Truncation
Depth (m)
-1000
-2000
-3000
-4000
-5000
SW3
SW4
SW2
SW2
SW-facing ramp
LW-facing ramp
SW-facing ramp
SW-facing ramp
Flamingo platform
Base-salt local high-W
0
2000 m
CGG
(b)
SW
NE
Scarp
RSB
RSB
RSB
SW2
SC1
Flamingo platform
BW-facing ramp
LW-facing ramp
SW-facing ramp
SW-facing ramp
SW-facing ramp
SW-facing ramp
Base-salt local high-X
0
2000 m
CGG
(c)
SW
NE
Scarp
RSB
RSB
RSB
SW2
SC1
Flamingo platform
SW-facing ramp
LW-facing ramp
SW-facing ramp
BW-facing ramp
Base-salt local high-Y
0
2000 m
CGG
Legend:
Seabed
Top Late Miocene
Top Middle Miocene
Top Early Miocene
Top Oligocene
Top Eocene
Top Albian
Top Salt
Base Salt
Primary Weld

Figure 8

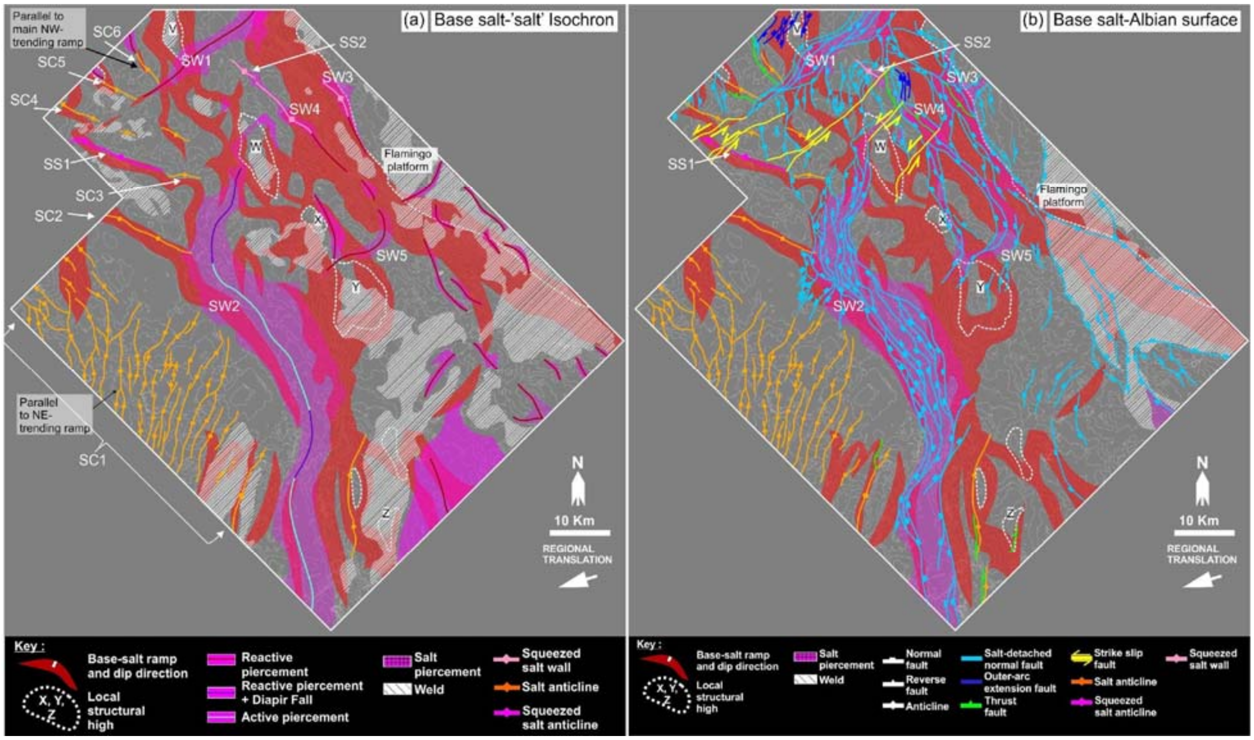

(a) Base salt-'salt' Isochron
Parallel to main NW-trending ramp
SC6
SC5
SC4
SS1
SC3
SC2
SW1
SS2
SW3
SW4
W
X
Y
Z
Flamingo platform
SW5
SW2
Parallel to NE-trending ramp
SC1
N
10 Km
REGIONAL TRANSLATION
Key :
Base-salt ramp and dip direction
Local structural high
Reactive piercement
Reactive piercement + Diapir Fall
Active piercement
Salt piercement
Weld
Squeezed salt wall
Salt anticline
Squeezed salt anticline
(b) Base salt-Albian surface
SW1
SS2
SW3
SW4
SS1
W
X
Y
Z
Flamingo platform
SW5
SW2
N
10 Km
REGIONAL TRANSLATION
Key :
Base-salt ramp and dip direction
Local structural high
Salt piercement
Weld
Normal fault
Reverse fault
Anticline
Salt-detached normal fault
Outer-arc extension fault
Thrust fault
Strike slip fault
Salt anticline
Squeezed salt anticline
Squeezed salt wall

Figure 9

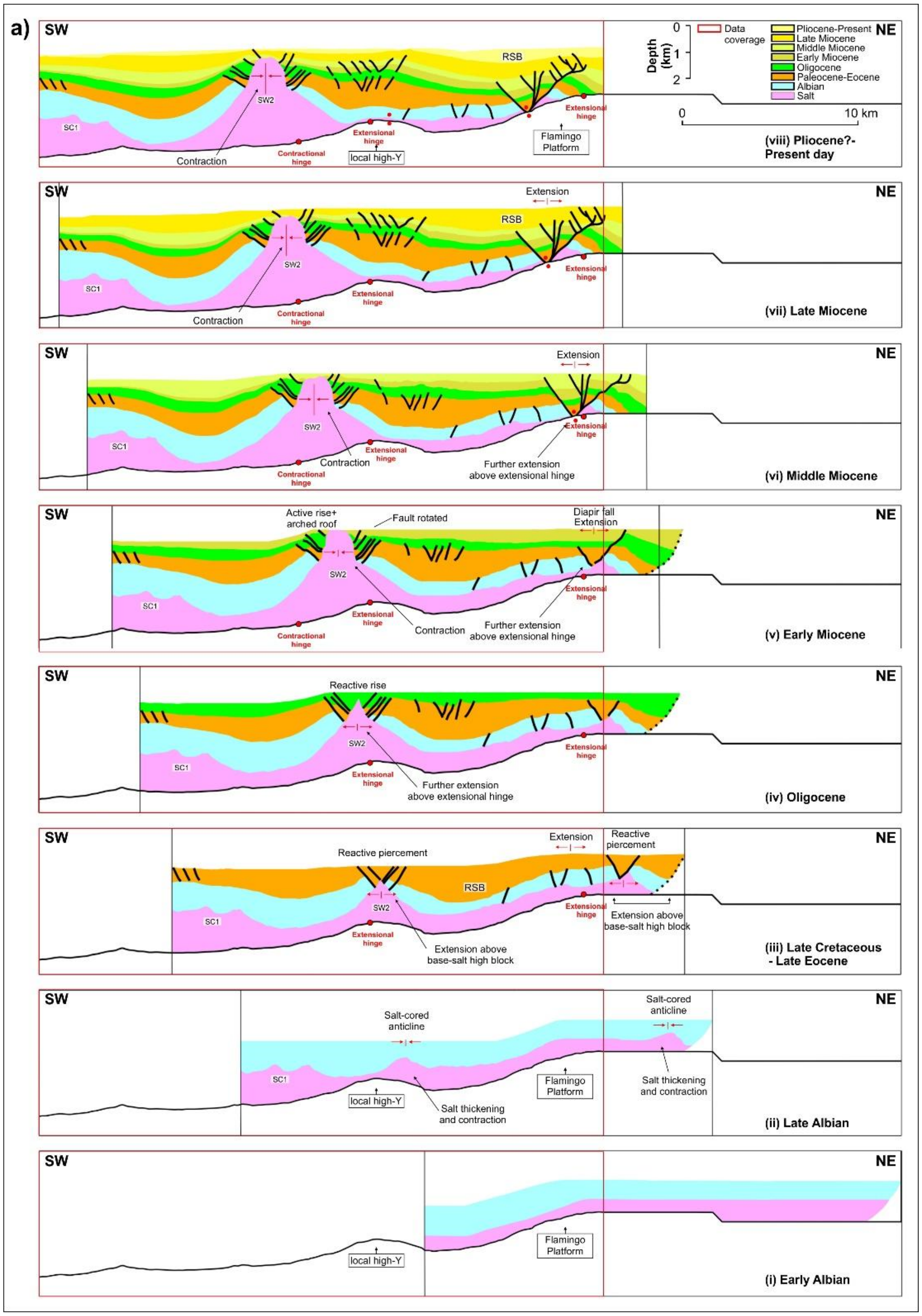

a)
SW
NE
Depth (km)
Data coverage
Pliocene-Present
Late Miocene
Middle Miocene
Early Miocene
Oligocene
Paleocene-Eocene
Albian
Salt
10 km
RSB
SW2
SC1
Contraction
Contractional hinge
Extensional hinge
local high-Y
Flamingo Platform
(viii) Pliocene?-Present day
Extension
(vii) Late Miocene
Further extension above extensional hinge
(vi) Middle Miocene
Active rise+ arched roof
Fault rotated
Diapir fall
(v) Early Miocene
Reactive rise
(iv) Oligocene
Reactive piercement
Extension above base-salt high block
(iii) Late Cretaceous - Late Eocene
Salt-cored anticline
Salt thickening and contraction
(ii) Late Albian
(i) Early Albian

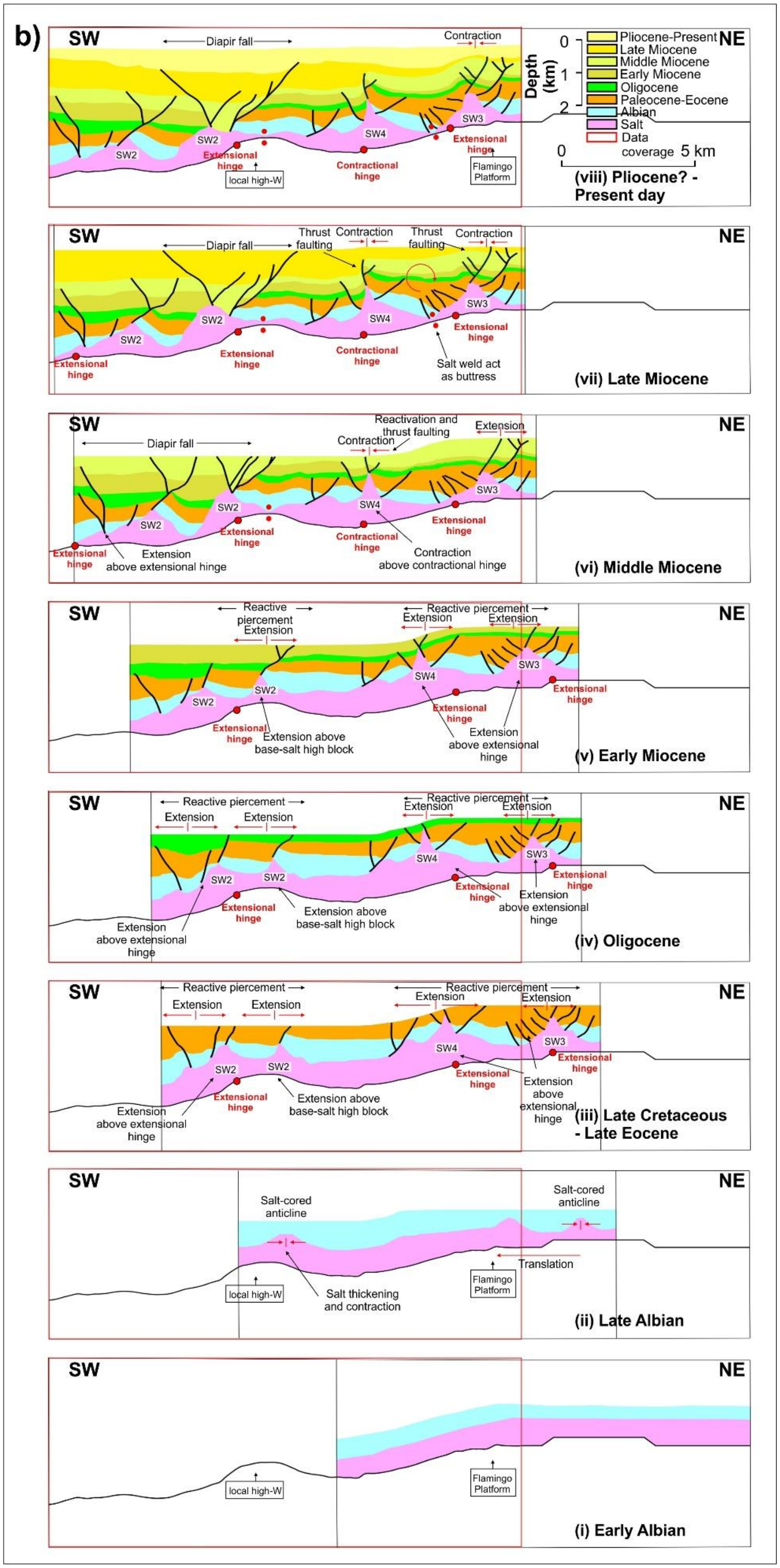

b)
SW
NE
Diapir fall
Contraction
Pliocene-Present
Late Miocene
Middle Miocene
Early Miocene
Oligocene
Paleocene-Eocene
Albian
Salt
Data coverage
Depth (km)
0
1
2
0
5 km
SW2
SW4
SW3
Extensional hinge
Contractional hinge
local high-W
Flamingo Platform
(viii) Pliocene? - Present day
Thrust faulting
Salt weld act as buttress
(vii) Late Miocene
Reactivation and thrust faulting
Extension
Extension above extensional hinge
Contraction above contractional hinge
(vi) Middle Miocene
Reactive piercement
Extension above base-salt high block
(v) Early Miocene
(iv) Oligocene
(iii) Late Cretaceous - Late Eocene
Salt-cored anticline
Salt thickening and contraction
Translation
(ii) Late Albian
(i) Early Albian

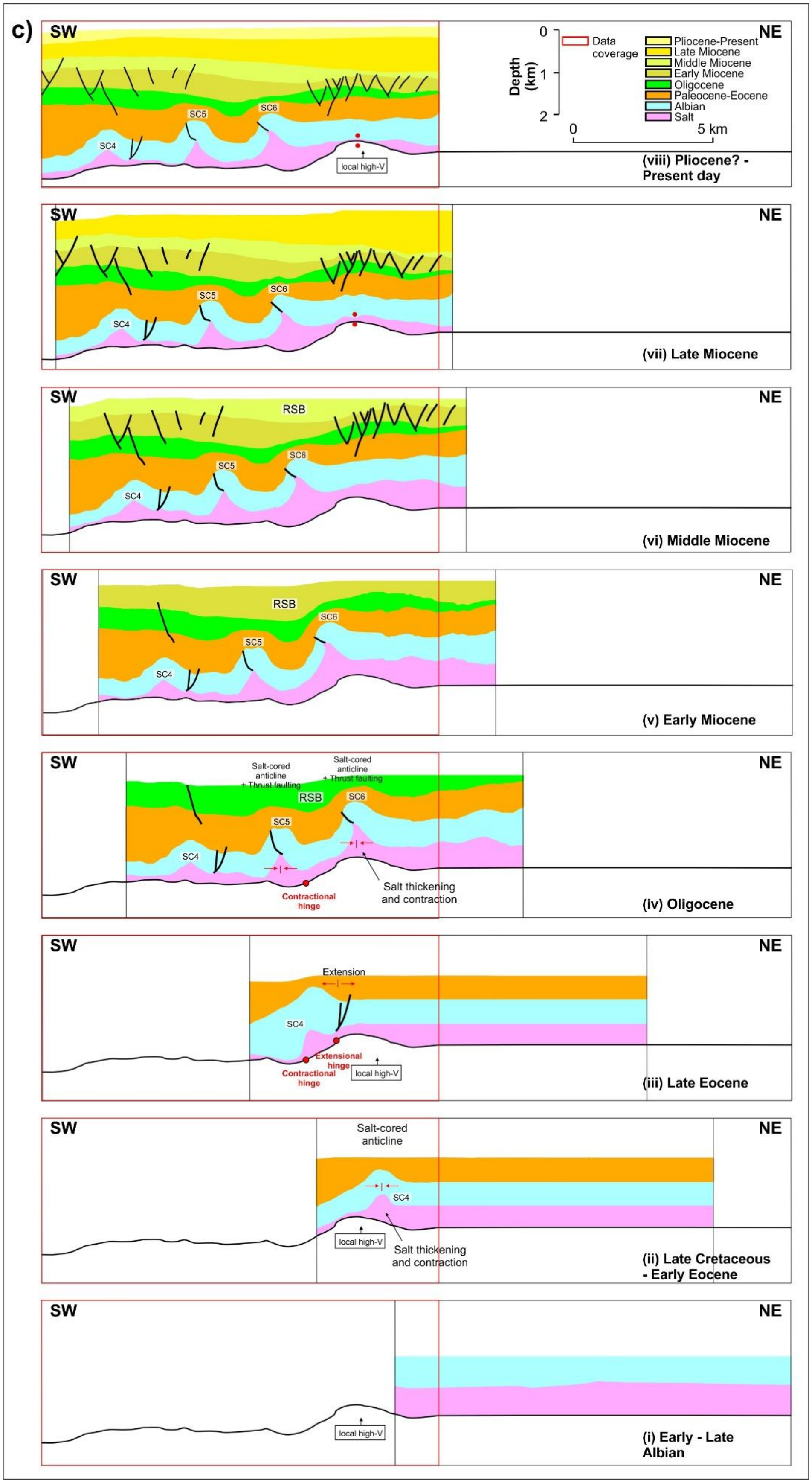

c)
SW
NE
Depth (km)
0
1
2
Data coverage
Pliocene-Present
Late Miocene
Middle Miocene
Early Miocene
Oligocene
Paleocene-Eocene
Albian
Salt
0
5 km
SC4
SC5
SC6
local high-V
(viii) Pliocene? - Present day
(vii) Late Miocene
RSB
(vi) Middle Miocene
(v) Early Miocene
Salt-cored anticline + Thrust faulting
Salt-cored anticline + Thrust faulting
Contractional hinge
Salt thickening and contraction
(iv) Oligocene
Extension
Extensional hinge
Contractional hinge
(iii) Late Eocene
Salt-cored anticline
Salt thickening and contraction
(ii) Late Cretaceous - Early Eocene
(i) Early - Late Albian

Figure 10

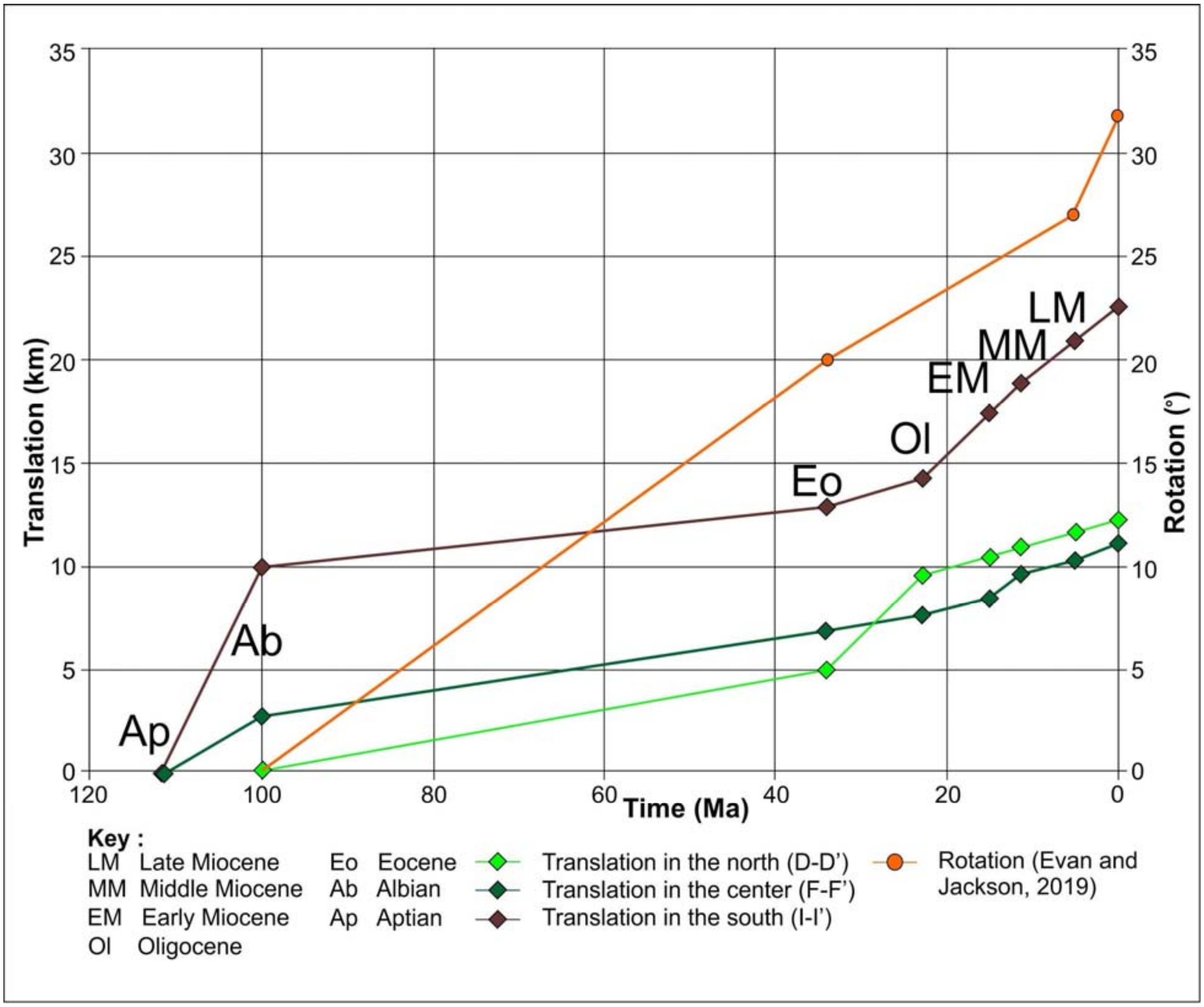

Translation (km)
Rotation (°)
Time (Ma)
Ap
Ab
Eo
Ol
EM
MM
LM
Key :
LM Late Miocene
MM Middle Miocene
EM Early Miocene
Ol Oligocene
Eo Eocene
Ab Albian
Ap Aptian
Translation in the north (D-D')
Translation in the center (F-F')
Translation in the south (I-I')
Rotation (Evan and Jackson, 2019)

Figure 11

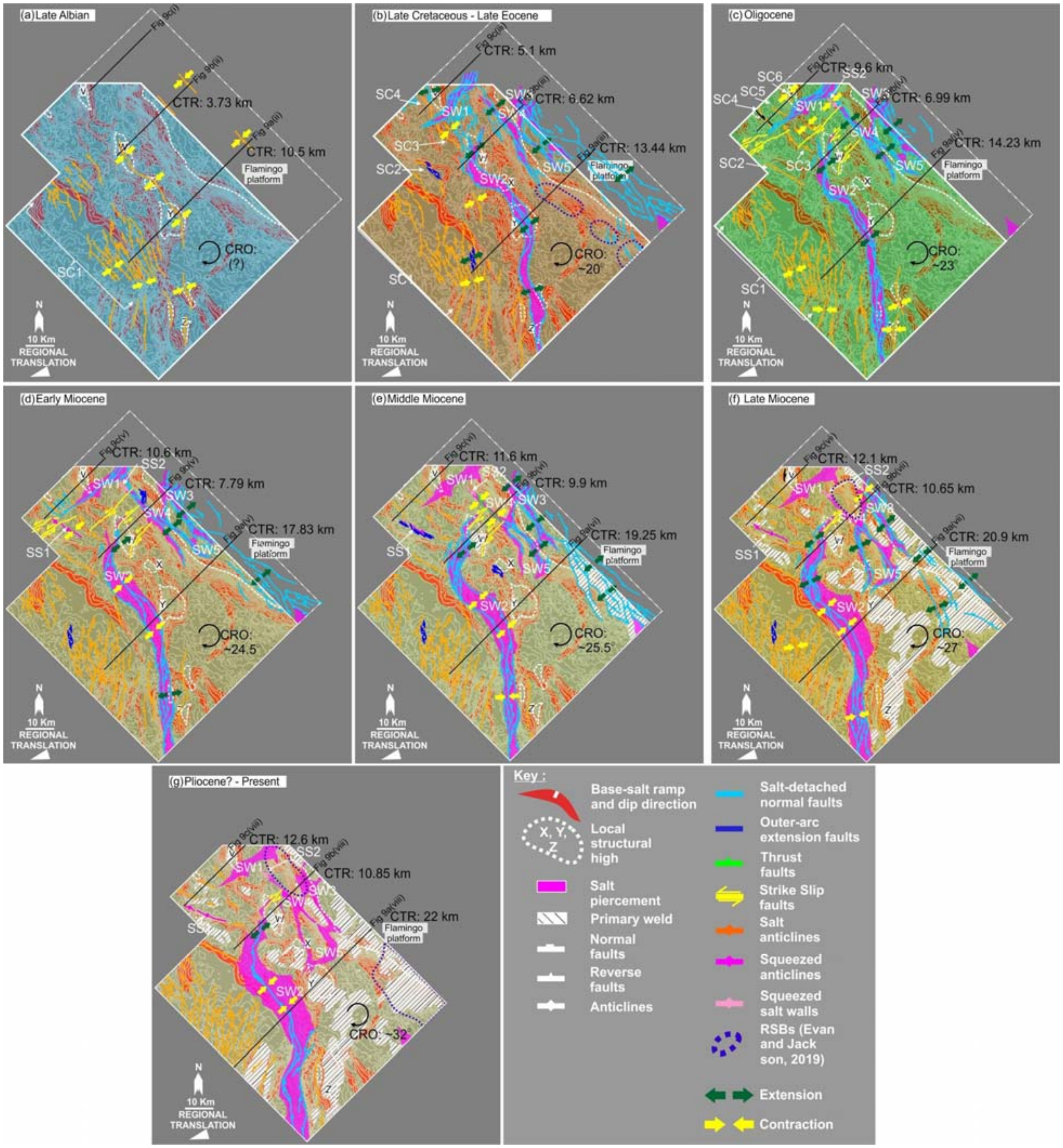

(a) Late Albian
CTR: 3.73 km
CTR: 10.5 km
Flamingo platform
SC1
CRO: (?)
(b) Late Cretaceous - Late Eocene
CTR: 5.1 km
CTR: 6.62 km
CTR: 13.44 km
SC4
SC3
SC2
SW1
SW2
SW5
CRO: ~20°
(c) Oligocene
CTR: 9.6 km
CTR: 6.99 km
CTR: 14.23 km
SC6
SC5
SS2
CRO: ~23°
(d) Early Miocene
CTR: 10.6 km
CTR: 7.79 km
CTR: 17.83 km
SS1
CRO: ~24.5°
(e) Middle Miocene
CTR: 11.6 km
CTR: 9.9 km
CTR: 19.25 km
CRO: ~25.5°
(f) Late Miocene
CTR: 12.1 km
CTR: 10.65 km
CTR: 20.9 km
CRO: ~27°
(g) Pliocene? - Present
CTR: 12.6 km
CTR: 10.85 km
CTR: 22 km
CRO: ~32°
10 Km
REGIONAL TRANSLATION
Key :
Base-salt ramp and dip direction
Local structural high
Salt piercement
Primary weld
Normal faults
Reverse faults
Anticlines
Salt-detached normal faults
Outer-arc extension faults
Thrust faults
Strike Slip faults
Salt anticlines
Squeezed anticlines
Squeezed salt walls
RSBs (Evan and Jack son, 2019)
Extension
Contraction

Figure 12: Physical model of Dooley et al (2018) (Not display, waiting for permission).